TM: Robert F. Fellows

Prepared for

NATIONAL AERONAUTICS AND SPACE ADMINISTRATION
Headquarters
Washington, D. C. 20546

by

Dr. F. F. Marmo, Project Director and
Principal Investigator

October 1969

EXPERIMENTAL AND THEORETICAL STUDIES IN PLANETARY AERONOMY

Quarterly Progress Report
Covering the Period 1 June 1969
through 30 August 1969

Prepared under Contract No. NASw-1726

I. INTRODUCTION

This fifth Quarterly Progress Report describes the technical progress achieved from 1 June 1969 through 30 August 1969 under NASA contract No. NASw-1726. Scientific investigation accomplished during this reporting period resulted in the generation of the following papers submitted, accepted and/or published in accredited scientific journals.

Technical Papers Submitted, Accepted and/or Published

a. Submitted:

Carbon Atoms in the Upper Atmosphere of Venus (F. Marmo and A. Engelman)	ICARUS

b. Accepted:

Line Broadening in Photoelectron Spectroscopy (J. A. R. Samson)	Rev. Sci. Instr.
On the Measurement of Rayleigh Scattering (J. A. R. Samson)	J. Quant. Spectrosc. & Radiat. Transfer
Vacuum Ultraviolet Absorption Cross Sections of CO, HCℓ, and ICN between 1050 and 2100Å (J. Myer and J. Samson)	J. Chem. Phys.

c. Published:

Electron Impact Excitation of the Dayglow (A. Dalgarno)	J. Atmos. Sci. 26, #4, 753 (1969).
Heats of Formation of CHO^+ and $C_3H_3^+$ by Photoionization (C. Matthews & P. Warneck)	J. Chem. Phys.

In Section II, technical summaries are presented on the work performed during the current reporting period. In compliance with the requirements

of the contract, an integrated tabulation by labor category and grade of total hours expended in the execution of the contract, for the specified reported time interval, is included in Section III.

II. SUMMARY OF TECHNICAL WORK PERFORMED FOR THE PERIOD 1 JUNE 1969 THROUGH 30 AUGUST 1969

The technical progress accomplished during the current reporting period can be conveniently described in terms of the two major categories contained in the statement of work: (A) laboratory studies, and (B) theoretical studies.

A. LABORATORY STUDIES

In accordance with the subject work statement it is required to perform the following laboratory investigations on selected planetary atmospheric gases: (1) an assessment on the precise determination of ionization potentials of molecules, and (2) ion molecule reactions in hydrocarbon systems. The results of these investigations are briefly discussed below.

(1) Ionization Potentials of Molecules

Precise values for the ionization potentials of molecules are essential for an accurate description of the state of ionization of a planetary atmosphere. For example, until recently the ionization potential of O_2 was taken to be 1026.5 $\pm$ 1 Å. With this error limit is was questionable whether the intense solar line of hydrogen at 1025.722Å could ionize O_2 in the earth's atmosphere. This problem was resolved under the present program (GCA Technical Report No. 65-30-N); a value of 1027.8 $\pm$ 0.1Å being obtained.

The most precise method for obtaining the ionization potential of a gas is the spectroscopic method. A series of Rydberg states must be identified and the limit of such a series gives the so-called "adiabatic" ionization potential. That is, the energy of the series limit represents the energy between the ground state of the molecule (with v" = 0 and J" = 0), and the specific electronic state of the ion (v' = 0 and J' = 0). The Rydberg formula is

$$T_o(n) = T_o(\infty) - \left[\frac{109737.31}{(n - \delta)^2}\right] \text{cm}^{-1} \qquad (1)$$

where $T_o(n)$ is the observed term value or wavenumber of the n^{th} Rydberg state. The subscript zero refers to a transition to v' = 0. $T_o(\infty)$ is the limit of the series $n \to \infty$ and represents the removal of an electron, that is, the ionization potential of the molecule. The quantity δ is called the quantum defect and represents the deviation of the molecular Rydberg series from the ideal case of atomic hydrogen. The constant 109737 cm^{-1} is the Rydberg constant for an infinite mass (R_∞). The most precise value of this constant is given by Cohen, et al.[1] as

$$R_\infty = 109737.31 \text{ cm}^{-1}.$$

This value differs by 0.007 cm^{-1} from the 1941 value[2] and by 0.001 cm^{-1} from the 1955 value.[3] This deviation is insignificant and does not affect the series limits previously published. The main error in determining the series limit lies in the ability to measure the term values $T_o(n)$ accurately. Errors in $T_o(n)$ typically lie between 1 and 100 cm^{-1}.

Although spectroscopic values provide the most precise values of the ionization potential large errors have been propagated in the literature because an author will often take the wavelength of a series limit expressed in electron volts from the original publication and convert this value to a wavelength expressed in angstroms. Unfortunately, the conversion factor used in the original publication is generally different from that used by a later author to convert electron volts back to angstroms. In some cases an author may report his results in electron volts but omit recording his conversion factor. It is perhaps useful then to tabulate the various values of this conversion factor as it has appeared in the past (see Table 1).

Another spectroscopic technique used for the determination of ionization potentials is the cyclic method, namely,

$$I\ (AB) = I\ (A) + D_o\ (AB) - D_o\ (AB^+), \qquad (2)$$

or

$$I\ (AB) = I'\ (AB) - h\nu \quad \text{(emission)} \qquad (3)$$

where I (AB) represents the first ionization potential of the molecule AB, I' (AB) represents a high ionization potential, and I (A) is the ionization potential of the atom A. $D_o(AB)$ and $D_o(AB^+)$ are the dissociation energies of the neutral molecule and of the ion, respectively,

TABLE 1

Conversion Factor to Convert Electron Volts to Angstroms

as reported since 1929

$V\lambda$ (eV Å)	Year	Reference
12336.1 ± 5.00	1929	a
12395.4 ± 2.10	1941	b
12397.80 ± 0.50	1953	c
12397.67 ± 0.22	1955	d
12398.10 ± 0.13	1965	e

(a) R. T. Birge, Revs. Mod. Phys. 1, 1 (1929)

(b) R. T. Birge, Revs. Mod. Phys. 13, 233 (1941).

(c) J. W. M. DuMond and E. R. Cohen, Revs. Mod. Phys. 25, 691 (1953).

(d) E. R. Cohen, J. W. M. DuMond, T. W. Layton and J. S. Rollet, Rev. Mod. Phys. 27, 363 (1955).

(e) E. R. Cohen and J. W. M. DuMond, Revs. Mod. Phys. 37, 537 (1965).

while $h\nu$ (emission) represents the energy of the radiation observed in emission of the (0,0) transition between the electronic states of the ion represented by I (AB) and I' (AB). Equations (2) and (3) are depicted schematically in Figure 1.

It is not always possible to identify Rydberg series in an absorption spectrum. For example, no such series has yet been observed leading to the first ionization potential of O_2. This is particularly true for higher ionization potentials of more complex molecules. Where no spectroscopic values exist the technique of electron and photon ionization has proved extremely valuable in providing ionization potentials. Further, the electron and photon impact method has provided checks on the reality of Rydberg series limits.

A critical review of the NO molecule is given below. The preferred energies of the first and high ionization potentials of NO are tabulated.

Owing to the complex absorption spectrum of nitric oxide, it is difficult to observe a Rydberg series leading to the first ionization potential of the molecule.

Electron impact methods were the first to be used to determine the first ionization potential of nitric oxide. Values ranged from 9.4 eV to the more accurate value of 9.25 eV.[4-6]

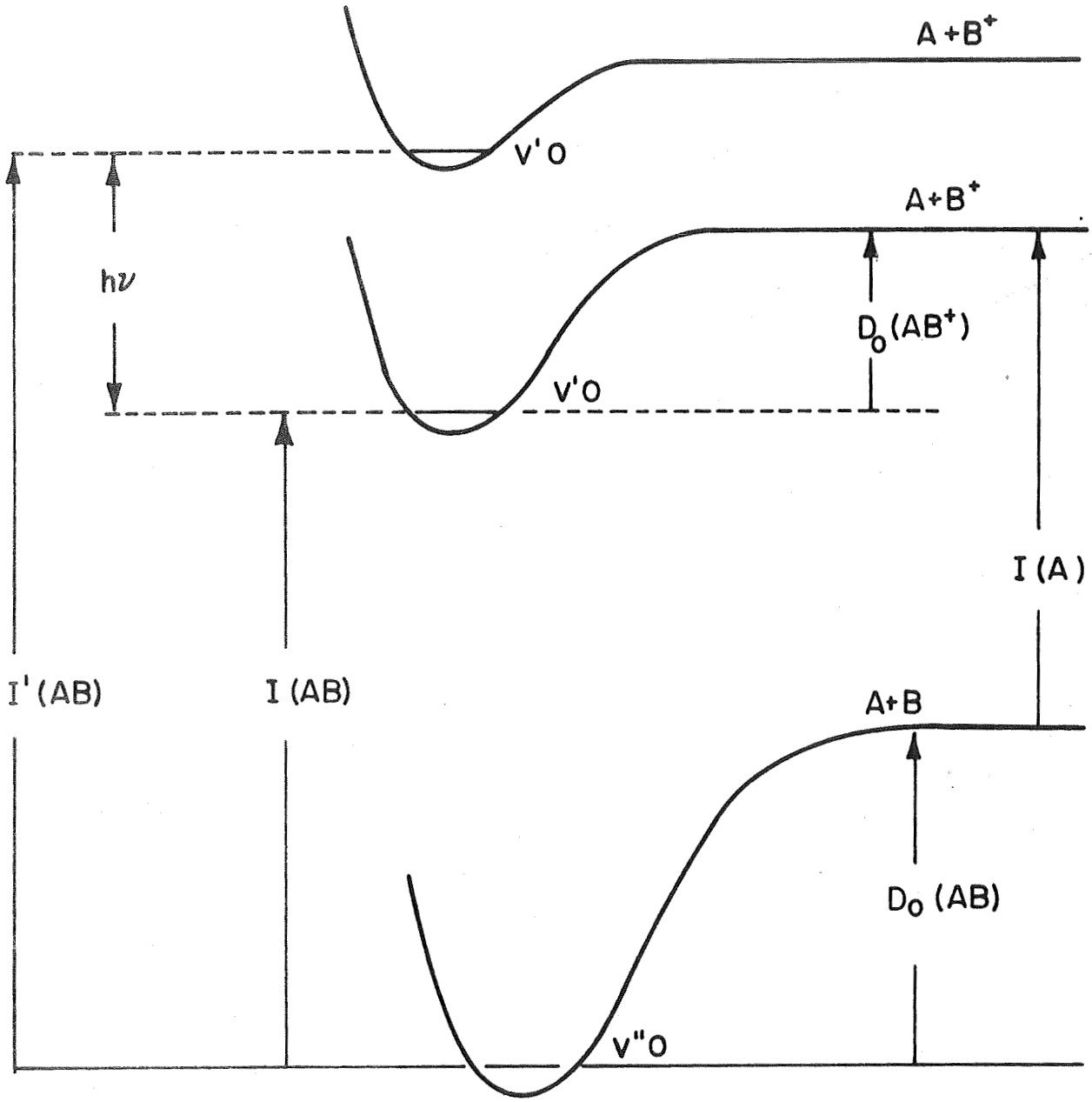

Figure 1. Potential energy curves for the molecule AB illustrating the energy relations used in determining the ionization potential (I (AB) of the molecule. Zero energy is taken at the v = 0 vibrational level of the ground state of AB.

The earliest determination of the first ionization potential using the technique of photoionization was by Watanabe, et al.[7] They reported a value of 9.20 eV. More accurate measurements by Watanabe[8] and by Nicholson[9] gave values of 9.253 eV ± 20 mV and 9.250 eV ± 5 mV, respectively.

A value of 9.267 eV ± 5 mV is obtained from the cyclical method using the differences in various term values determined spectroscopically. Baer and Miescher[10,11] and Tanaka[12] observed an emission system of NO from the A $^1\Pi$ state to the ground X $^1\Sigma^+$ state of the ion. Both groups gave a value of 73083.9 cm^{-1} for the energy separation between the v = 0 levels of each state. Subtracting this value from the energy of the A $^1\Pi$ state above the ground state of the molecule as determined by Tanaka[13] and Huber[14] we get 9.216 eV and 9.267 eV, respectively.

As mentioned at the beginning of this discussion, the absorption spectrum of NO is complex. However, a Rydberg series has finally been identified by Dressler and Miescher[15] leading to the first ionization potential. A value of 9.266 eV ± 8 mV was obtained and is considered to be the most accurate value. Miescher has observed two other Rydberg series which also approach the above limiting value.[16]

The reason for the apparent discrepancy between spectroscopic and photoionization values of the first ionization potential is that in the photoionization technique the ionization potential is usually taken as the energy at which the first ions appear. In the case of nitric oxide, however, the neutral molecules exist not only in the ground X $^2\Pi_{1/2}$ state,

but some exist in the X $^2\Pi_{3/2}$ state which lies 0.015 eV above the ground state. At room temperature (300°K) there should be 1.8 times as many molecules in the excited state as exist in the ground state. Since direct photoionization takes place for molecules in both states, the appearance potential of ions is lowered by 0.015 eV. The population of rotational states further decreases the appearance potential by 0.003 eV, according to Dressler and Miescher.[15] Thus, the photoionization values should be about 0.018 eV lower than the spectroscopic values; and this is indeed the case.

Higher ionization potentials have been obtained spectroscopically[13,14] and by the technique of photoelectron spectroscopy.[17-19] Three Rydberg series have been identified and called by Tanaka the α, β, and γ series converging to limits of 14.226, 16.563, and 18.316 eV, respectively. However, the α series is not confirmed by photoelectron spectroscopy and must be considered to be in error. Huber[20] has attempted to classify the excited electronic states of NO^+ while Lefebvre-Brion and Moser[21] have predicted the order of the states using approximate Hartree-Fock orbitals for the ground state of the ion.

Table 2 lists the preferred ionization potentials of NO expressed in units of reciprocal centimeters, angstroms, and electron volts. The spectroscopic values obtained by Huber for the β and γ series limit are listed because of their consistency with the Baer-Miescher bands to provide a first ionization potential in agreement with the Rydberg analysis of Dressler and Miescher.

TABLE 2

FIRST AND HIGHER IONIZATION POTENTIALS OF NITRIC OXIDE

State	Ionization Potential (cm^{-1})	(Å)	(eV)	References
X $^1\Sigma^+$	74 740 ± 60	1338 ± 1	9.266 ± 0.008	(12) S
a $^3\Sigma^+$	126 230	792.2	15.65	(15) PE
$^3\Pi$	133 550 ± 10	748.78 ± 0.06	16.558 ± 0.001	(11) S
A $^1\Pi$	147 830 ± 40	676.45 ± 0.18	18.328 ± 0.005	(11) S
?	175 190 ± 70	570.8 ± 0.3	21.72 ± 0.01	(16) PE

S = Spectroscopy

PE = Photoelectron Spectroscopy

(2) Ion-Molecule Reactions in Hydrocarbon Systems

From spectroscopic observations, it is known that the Jovian planets contain appreciable amounts of methane and ammonia in their atmospheres, in addition to hydrogen and helium. McNesby[22] recently has studied the photochemistry of such a system and has shown that, with hydrogen in excess, the first order photodissociation products of methane and ammonia essentially recombine, resulting in no net change of the system except to heat the atmosphere. Nevertheless, a small amount of higher hydrocarbons would be formed as a second order perturbation. For example, Sagan[23] has argued for the formation of adenine and other amino products. With this background, it becomes of interest to investigate ion reactions involving hydrocarbons. A great number of such reactions has been studied in the past with conventional electron impact mass spectrometers. With the applied techniques, these investigations have been complicated by the many ions produced simultaneously in the ion source, and their reactions with the parent gas. It appears, that the photoionization mass spectrometer technique, by virtue of the selective ionization processes involved, can reduce the complexities of the reaction system sufficiently to allow a less ambiguous analysis of the data.

On this basis, we have studied ion reactions in the systems ethylene-acetylene, acetylene-methane and methane-ethylene. The results have already led to some interesting conclusions, although all the data have not yet been analyzed, and a detailed evaluation of those data which have been analyzed has not yet been possible. The results presently available, and their implications will be discussed below.

The techniques employed in this study have been described in detail previously.[24] Briefly, the apparatus involved a 180 degree magnetic mass spectrometer with conventional ion source geometry and electronic multiplier. Ions are produced by extreme UV radiation generated in a repetitive spark light source. A Seya monochromator provides wavelength isolation with a spectral resolution of about 5Å. The light beam transversed the ion chamber midway between the repeller plate and the ion exit orifice which were placed 0.6 cm apart. The repeller potential was one volt. The gas pressure in the ion source was measured with a McLeod gauge through the hollow stem of the repeller.

Reactions were investigated in the low pressure domain where the motion of ions is mainly acceleration in the repeller field. Products were assessed from the appearance of new peaks as the pressure in the ion chamber was raised. Rate coefficients were determined from the decrease of the primary ion intensity as a function of the gas pressure, or as a function of the partial pressure of an added second gaseous component; and from the residence time of the primary ions in the source chamber. Residence times were determined from the time delay of the ion pulse arriving at the mass spectrometer collector after the deposition of ions in the source by the light pulse. As described previously, delay times were measured for several repeller potentials and a graphical extrapolation toward infinite repeller potential is used to separate the ion source residence time from the total flight time of the ions in the mass spectrometer. In the present experiments the half-rise time of the integrated ion pulse was utilized for reference in the delay time measurements so that averaged residence times were obtained.

In the following, results will be presented for ion-molecule reaction in ethylene, acetylene, and their mixtures. At ionizing wavelengths above 945 Å, up to the ionization threshold, the primary photoionization products in both ethylene and acetylene are the parent ions $C_2H_4^+$ and $C_2H_2^+$, respectively, and other ions are formed only by secondary reactions of these ionic species. In the wavelength region 900-945 Å, photoionization of acetylene still yields only the parent ion, whereas that of ethylene produces $C_2H_2^+$ in addition to $C_2H_4^+$. This latter wavelength region thus facilitates a study of the reactions of $C_2H_2^+$ with ethylene in the absence of interference by acetylene. The present investigation made use of radiation at 1087Å and 923Å both provided by operating the spark source with nitrogen.

The development of the ion spectrum with pressure when acetylene is ionized at 1087Å is shown in Figure 2. The important product ions appear at mass numbers 50, 51 and 52. The reaction paths responsible for the production of these ions are

$$\begin{aligned} C_2H_2^+ + C_2H_2 &\rightarrow C_4H_2^+ + \text{products} \\ &\rightarrow C_4H_3^+ + \text{products} \\ &\rightarrow C_4H_4^+ \end{aligned} \qquad (4)$$

At pressures below 10 microns, the product ratios are found to be constant. The determination of the average values for the branching ratios of reaction (4) gave 29% for the formation of $C_4H_2^+$, 66% for $C_4H_3^+$ and 5% for $C_4H_4^+$. The pressure dependence for the formation of the last ion is such

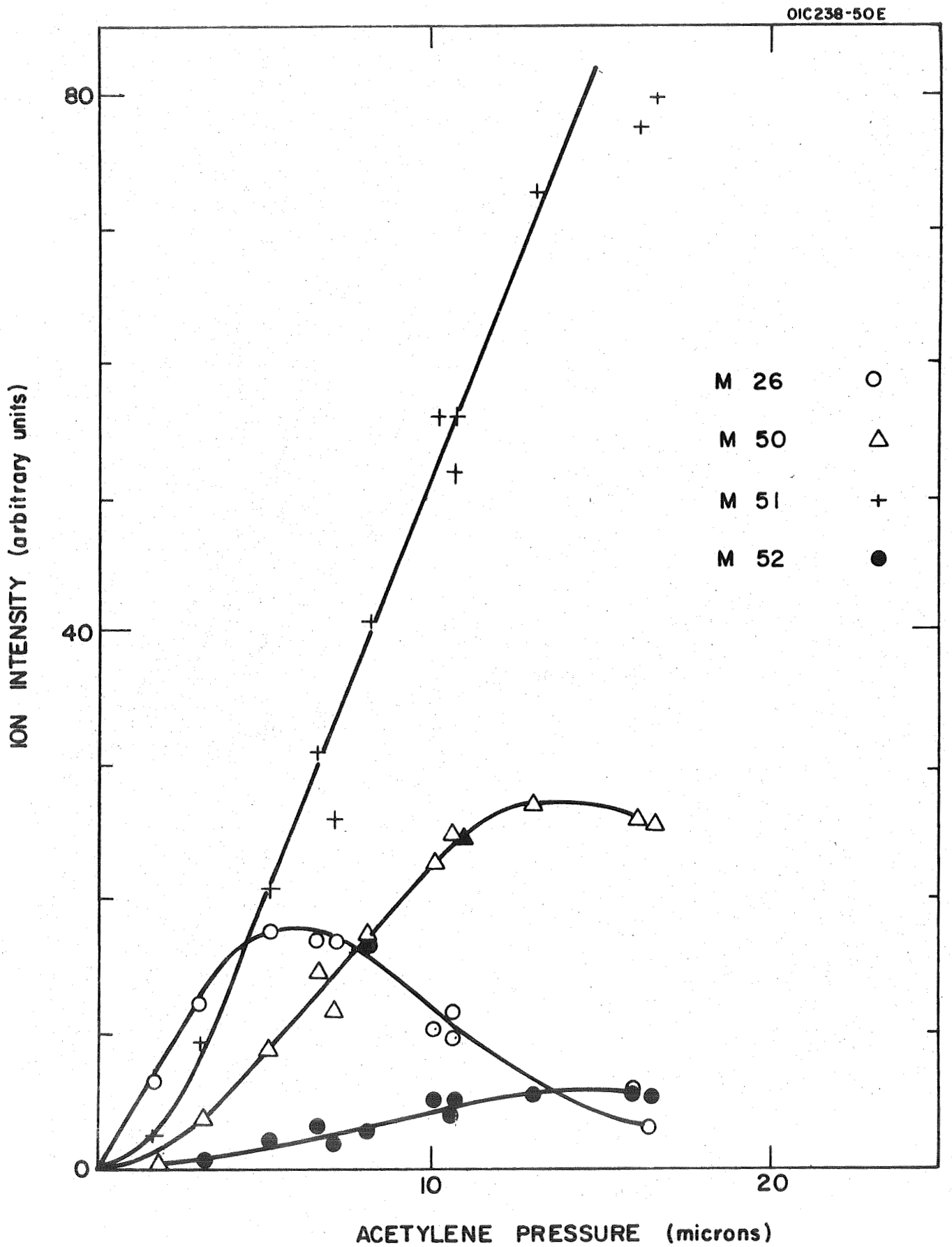

Figure 2. Intensities of major ions in acetylene as a function of pressure. Ionizing wavelength 1087Å.

that it precludes the participation of the third collision partner. The formation of $C_4H_4^+$ in a binary collision is possible only if the lifetime of the intermediate collision complex is sufficiently long, so that the collision complex is stabilized by subsequent collisions regardless of the pressure. Since the product branching ratio does not depend on the pressure, it must further be concluded that the other two products result from the same process as $C_4H_4^+$. Thus, the detailed mechanism of reaction (4) in the investigated pressure domain can be written as

$$C_2H_2^+ + C_2H_2 \rightarrow C_4H_4^{+*} \quad (4a)$$

$$C_4H_4^{+*} + C_2H_2 \rightarrow C_4H_2^+ + C_2H_4^* \quad (4b)$$
$$\rightarrow C_4H_3^+ + C_2H_3^*$$
$$\rightarrow C_4H_4^+$$

where the asteric denotes (vibrationally) excited species. The present results contain no information on the fate of the neutral products in reaction (4b), but a possible course is their dissociation to yield H_2 or H and acetylene.

At pressures greater than 10 microns, the ratio of products M50/M51 decreases and new ions appear at mass numbers 74, 75 and 76 due to the reactions

$$C_4H_2^+ + C_2H_2 \rightarrow C_6H_2^+ + H_2 \quad (5)$$
$$\rightarrow C_6H_3^+ + H$$

$$C_4H_3^+ + C_2H_2 \rightarrow C_6H_3^+ + H_2 \quad (6)$$
$$\rightarrow C_6H_4^+ + H$$

of these, reaction (5) predominates, producing $C_6H_2^+$ and $C_6H_3^+$ ions in approximately equal amounts. The sum of all the observed ion intensities, i.e. that of the acetylene and that of the various product ions, was found directly proportional to the acetylene pressure, indicating that reactions 4 through 7 account for essentially all the ions observed and further reactions are negligible. The rate coefficient for reaction (4) including all its channels can be derived from the decrease of the $C_2H_2^+$ ion intensity as a function of pressure from the relation

$$k = \frac{2.3}{\tau\, n} \log \frac{N_o}{N}$$

where τ is the average residence time of $C_2H_2^+$ in the ion source, n the number density of acetylene in the source, N_o is the sum of all ions taken equal to the initial $C_2H_2^+$ ion intensity and N is the measured $C_2H_2^+$ ion intensity. The average value of the rate coefficient thus determined for reaction (4) is $k_1 = 1.39 \times 10^{-9}$ cc/molecule sec. The value expected on the basis of the ion induced dipole interaction theory is $k_1(\text{theor.}) = 1.29 \times 10^{-9}$ cc/molecule sec. The experimental rate coefficient is found to agree with the theoretical one within experimental error.

Similar results were obtained for ion reactions in acetylene when the photoionizing wavelength was 923Å. Again, $C_2H_2^+$ was the only primary ion observed, and reaction (4) with its three channels was the major loss process for $C_2H_2^+$. The ratio of product channels was determined as $C_4H_2^+$ 29%, $C_4H_3^+$ 67%, $C_4H_4^+$ 4%. Within experimental error, these values are the same as those given above for the reaction when working with 1087Å radiation. Moreover, the associated rate coefficient

was found to be $k_1 = 1.38 \times 10^{-9}$ cc/molecule sec. This value agrees well with the value given above, and like that one is in accord with theoretical prediction. These results, therefore, show that the acetylene ion formed at 923Å behaves identically to that formed at 1087Å, even though it may be produced with some internal excitation.

The development of the spectrum of the major ions with pressure when ethylene is ionized at 1087Å is shown in Figure 3. The significant product ions appear at mass numbers 41 and 55. They are due to the reaction

$$\begin{aligned} C_2H_4^+ + C_2H_4 &\rightarrow C_3H_5^+ + CH_3 \\ &\rightarrow C_4H_7^+ + H \end{aligned} \qquad (7)$$

The branching ratio of this reaction is found to result to 90% in $C_3H_5^+$ ions, and to 10% in $C_4H_7^+$ ions. At pressures above about 10 microns, this ratio is perturbed by the strong increase of a tertiary product at mass 69 due to the condensation reaction

$$C_3H_5^+ + C_2H_4 \rightarrow C_5H_9^+ \qquad (8)$$

which consumes the $C_3H_5^+$ ions formed in reaction (4). The $C_4H_7^+$ ion formed in the reaction[25] also undergoes further reactions but these are significant only at pressures greater than 30 microns and even then their contribution to the total ion abundance is small. Contributions to the total ion spectrum were observed also on mass numbers 42 and 70, but they were too small to be taken into account in a meaningful way. However, they are observed with higher intensity in the photoionization of ethylene at 923Å and will be discussed further below.

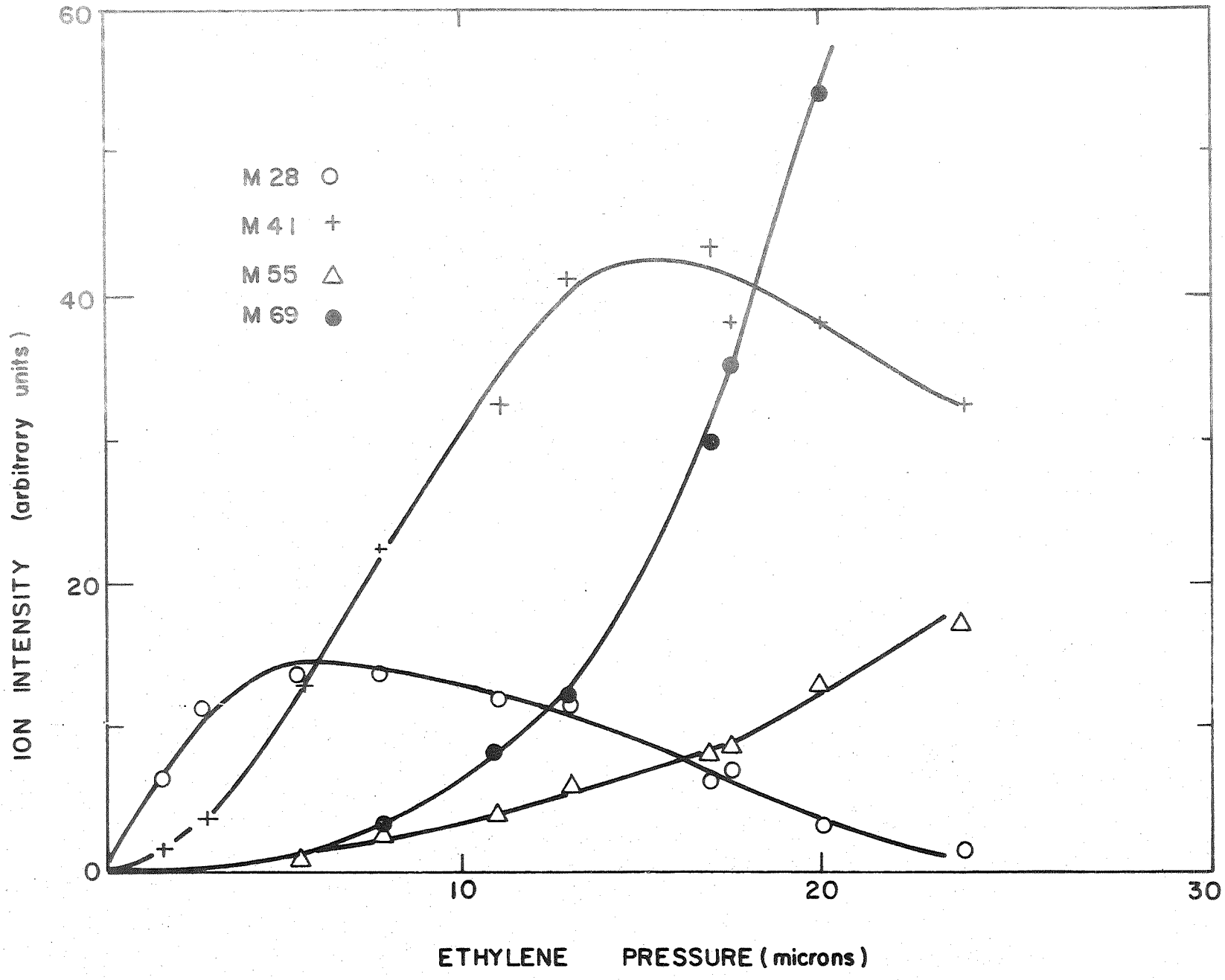

Figure 3. Intensities of major ions in ethylene as a function of pressure. Ionizing wavelength 1087Å.

As in acetylene, an association product, $C_4H_8^+$, was found in the photoionization of ethylene. However, compared to the behavior at the mass 54 ion in acetylene, the association product in ethylene showed a different pressure dependence. Figure 4 indicates that the ratio of the intensity of the mass 56 ion to the total product ion intensity is not constant but increases with pressure. The dependence on pressure is linear and the straight line obtained extrapolates to the origin of the plot. This is evidence that in contrast to the acetylene case, the association product of the ethylene ion is formed by a third body reaction

$$C_2H_4^+ + 2\ C_2H_4 \rightarrow C_4H_8^+ + C_2H_4 \qquad (9)$$

The rate coefficient for reaction (7) was determined from the decay of the $C_2H_4^+$ ion intensity compared to the total ion intensity. A value of $k_4 = 1.24 \times 10^{-9}$ cc/molecule sec was obtained. The rate coefficient calculated from the induced dipole moment theory is k_4(theor.) = 1.29×10^{-9}. As for the previous cases, the agreement between the experimental and the theoretical values is good. From the rate coefficient associated with reaction (7) and the data shown in Figure 4 the rate coefficient for reaction (9) can be derived as $k_6 = 1.5 \times 10^{-25}$ cc^2/molecule^2 sec. The magnitude of this value indicates that the average lifetime of the intermediate collision complex before it is stabilized by a third body collision is approximately 1×10^{-7} seconds. Since this rate coefficient is derived from a product intensity rather then the primary ion intensity decrease, it is probably not as reliable as the other rate coefficients. Nevertheless, the implied order of magnitude makes reaction (9) one of

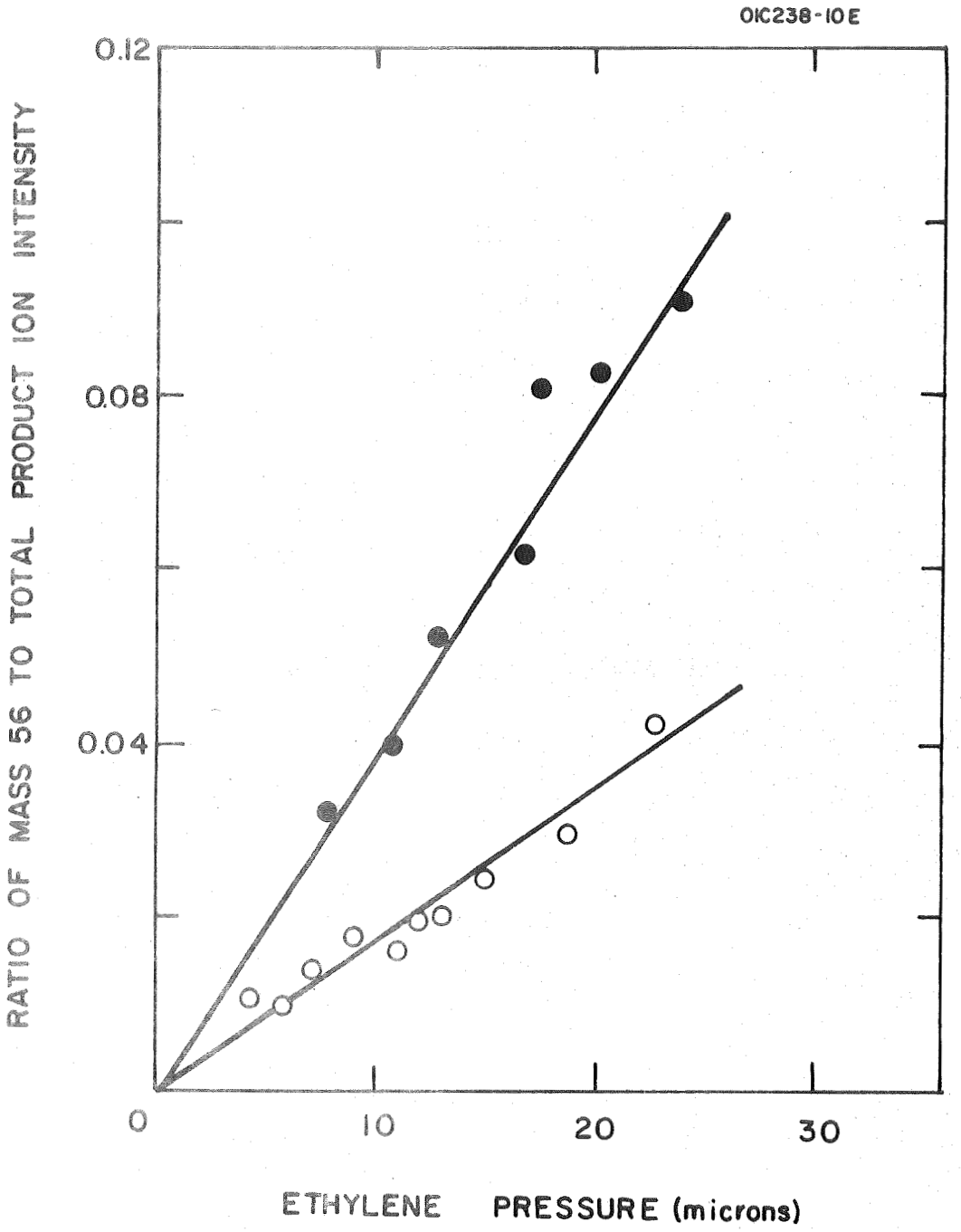

Figure 4. Ratio of Mass 56 ion intensity to total product ion intensity in ethylene as a function of pressure. Ionizing wavelength 1087Å: solid points; 923Å: open points.

the most rapid termolecular ion reactions. Gordon and Ausloos,[25] from studies of the photolysis of ethylene at 1048/66Å had concluded that formation of the butenes is due mainly to neutralization of the $C_4H_8^+$ ion produced by reaction (9).

Since the primary ions formed by photoionization of acetylene and ethylene with 1087Å radiation are only the parent ions of these gases, and their reactions have been established by the results reported above, it was of interest to look for additional reactions of these species in a mixture of ethylene and acetylene. Specifically, charge transfer from the acetylene ion to ethylene was expected to occur, as it is an exothermic process. In these experiments, therefore, acetylene was entered into the ion source chamber at a fixed rate providing a partial pressure of 3.8 microns, and ethylene was added in varying amounts at partial pressures up to 8 microns. In this pressure range, the ion intensities due to ethylene and its reaction products at mass number 28, 41 and 55 fitted well with the intensity curves shown in Figure 3 for pure ethylene so that the ethylene ions must react little or not at all with acetylene. The acetylene ion intensities, however, decreased considerably with increasing ethylene pressure as shown in Figure 5a indicating the occurrence of an interaction. At the same time new peaks appeared at mass numbers 39 and 53. Thus the reaction

$$C_2H_2^+ + C_2H_4 \rightarrow C_3H_3^+ + CH_3 \qquad (10)$$
$$\rightarrow C_4H_5^+ + H$$

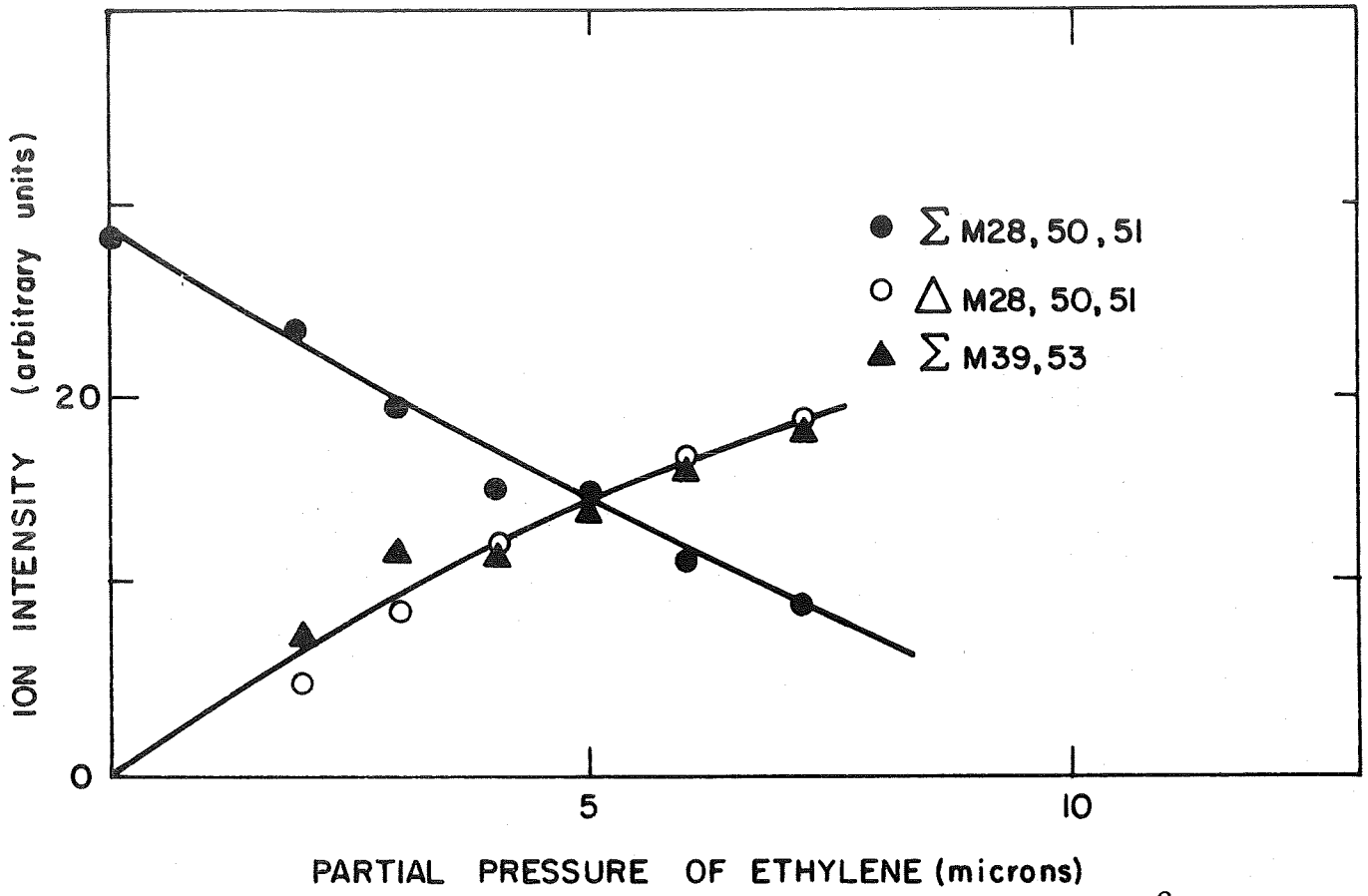

Figure 5. Photoionization of acetylene-ethylene mixture at 1087Å. Intensities of primary and product ions when ethylene is added to 3.8 microns of acetylene. (a) Loss of $C_2H_2^+$ and gain of $C_3H_3^+$ and $C_4H_5^+$ to show their equivalence. (b) Comparison of $C_2H_4^+$ and follow-on ion intensities (crosses) with those observed in pure ethylene (points) to show their equivalence.

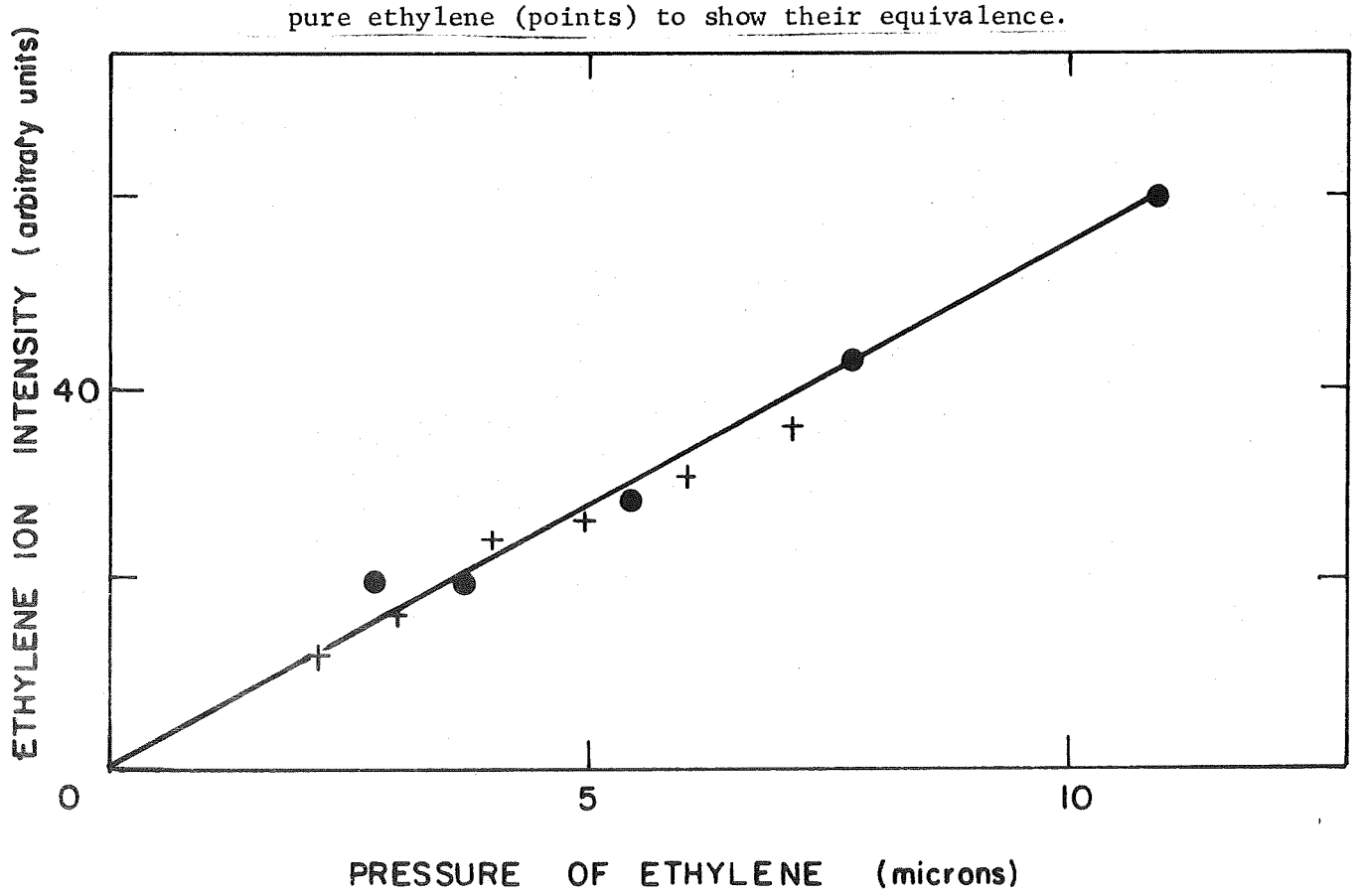

is indicated. From the intensity distribution of the ions M39 and M53 the branching probability for reaction (10) was obtained as $C_3H_3^+$ 71% and $C_4H_5^+$ 29%. The sum of the intensities of these products matched the losses of the acetylene ions within the experimental error (see Figure 5a) so that reaction (10) must be the major reaction that acetylene ions undergo with ethylene. Several previous workers[26] have concluded, however, that charge transfer is a major reaction channel. To investigate this problem further, the sum of the intensities of ions due $C_2H_4^+$ and its interaction with ethylene are plotted in Figure 5b for ethylene in the presence of acetylene and for ethylene alone. It is evident that both sets of data coincide, whereas if charge transfer took place to an appreciable extent, the total ethylene ion intensity should increase with increasing ethylene pressure. It may be agreed that the lack of an increase in the ethylene ion intensity is due to a reaction of these ions with acetylene and that charge transfer is operative nonetheless. The probability for this additional reaction would be greatest at low ethylene concentrations because then the concentration ratio of acetylene to ethylene is large. However, with increasing ethylene pressure the importance of this process diminishes in comparison with the interaction with ethylene, and the total ethylene ion intensity should increase correspondingly. From the failure to detect such an increase at the highest ethylene pressure involved ($C_2H_4/C_2H_2 = 2$), from the intensity losses of the acetylene ions, and from the corresponding increase of the M39 and M53 ion intensities shown in Figure 5a it is estimated that the charge transfer reaction

$$C_2H_2^+ + C_2H_4 \rightarrow C_2H_4^+ + C_2H_2 \qquad (11)$$

occurs to less than 15 percent of the overall reaction of acetylene ions.

From the decrease of the $C_2H_2^+$ ion intensity as the ethylene pressure is increased and from the measured residence time of the acetylene ions in the source chamber, the rate coefficient for the reaction (10) and (11) combined is found to be $k_{7+8} = 1.35 \times 10^{-9}$ cc/molecule sec. The rate coefficient calculated from theory is $k_{7+8}(\text{theor.}) = 1.31 \times 10^{-9}$ cc/molecule sec. Within the experimental error the values are identical.

When ethylene was photoionized with 923Å radiation, the major ion reactions were found to be reactions (7) through (10) discussed above, involving the primary ions $C_2H_4^+$ and $C_2H_2^+$. In accord with expectation, the major product ions appeared at mass numbers 41, 55, 56, and 69, and at 39 and 53 respectively. However, some additional reactions occurred also, as evidenced by signals on mass numbers 27, 29, 40, 42, 54, 67 and 70. Although the contribution of these ions amounted to no more than 7 percent of the total ion intensity, their assignment is required for a complete interpretation of the results. The M67 ion is taken to be the condensation product of $C_3H_3^+$ with ethylene, because it was present also in the 1087Å photoionization of an acetylene-ethylene mixture when the ethylene pressure exceeded 10 microns. The behavior of most of the other ions identifies them as product ions. By analogy to reactions (7), (8), and (10), therefore the signals on mass numbers 40 and 54 are assigned to products of M27, and the signals on mass numbers 42 and 70 are assigned to products of the ion M29. These assignments then reduce the problem of the minor ions to the origin of M27 and M29. The intensity of these

ions and their follow-on products is much greater than the expected isotope contributions in ethylene (mainly due to C^{13}), so that the M27 and M29 ions must be identified as $C_2H_3^+$ and $C_2H_5^+$. The give rise to the reactions

$$\begin{aligned} C_2H_3^+ + C_2H_4 &\rightarrow C_3H_4^+ + CH_3 \\ &\rightarrow C_4H_6^+ + H \end{aligned} \qquad (12)$$

From the M40 and M54 contributions the branching ratio of this reaction is found to yield $C_3H_4^+$ to about 60 percent and $C_4H_6^+$ to about 40 percent. Similarly, M42 and M70 are due to

$$\begin{aligned} C_2H_5^+ + C_2H_4 &\rightarrow C_3H_6^+ + CH_3 \\ &\rightarrow C_4H_8^+ + H \end{aligned} \qquad (13)$$

$$C_3H_6^+ + C_2H_4 \rightarrow C_5H_{10}^+ \qquad (14)$$

in analogy to reactions (7) and (8) the branching ratio of reaction (13) cannot be determined, because the $C_4H_8^+$ ion on mass number 56 coincides with the butene ion formed in reaction (9). It appears, however, from the pressure dependence of the M56 intensity that the contribution of reaction (13) to the mass 56 peak is almost negligible, so that the $C_3H_6^+$ formation in reaction (13) must be the predominant .

The M29 ion could be conceivably formed from an ethane impurity in ethylene, but since the M30 peak was absent, this possibility is excluded. The nature of the $C_2H_5^+$ ion indicates that it is a product ion, rather than a primary ion. However, the pressure dependence of the sum of the intensities of the M29 sequence is fairly linear as shown in Figure 6, whereas product intensities should show a quadratic pressure dependence

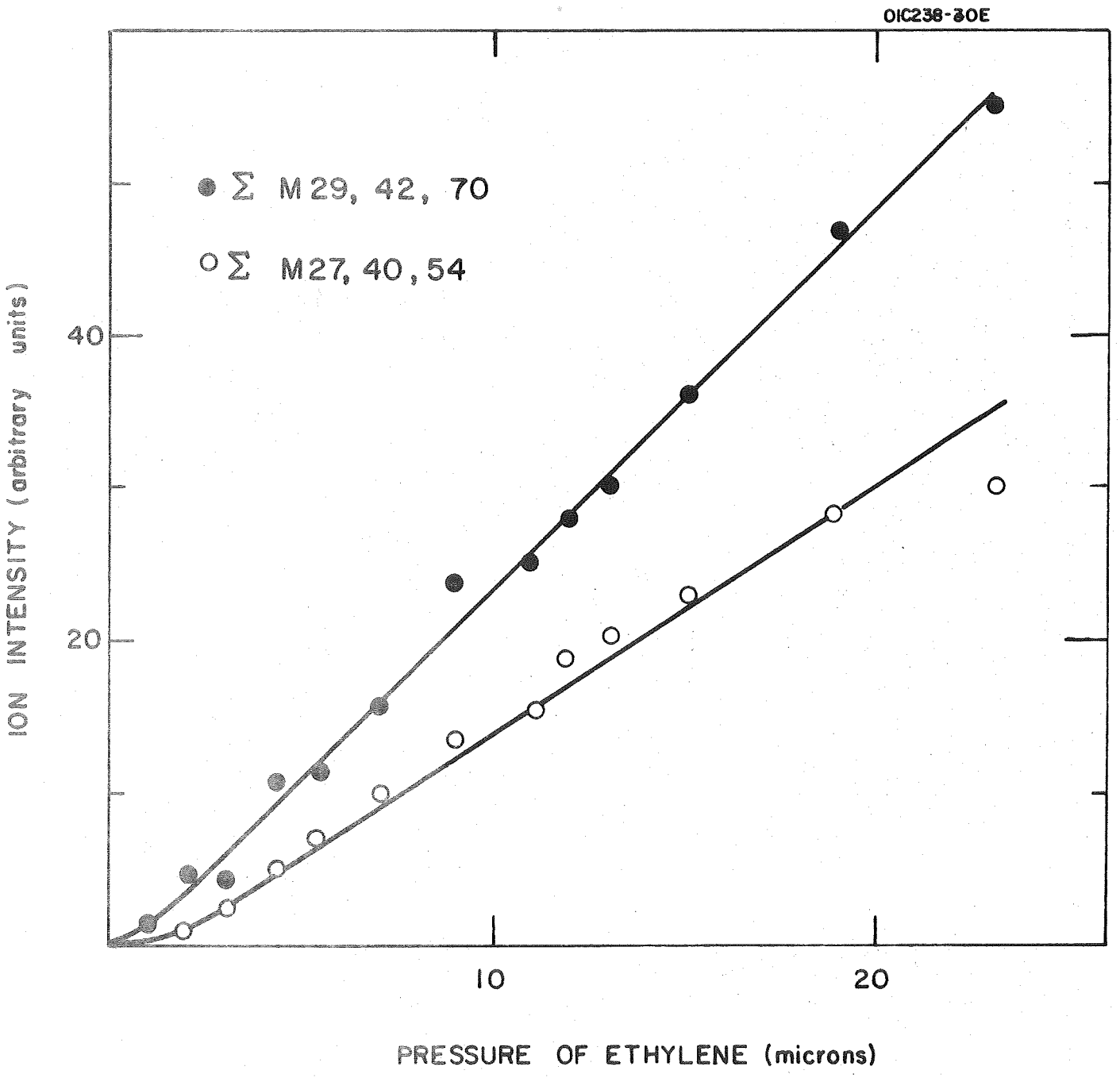

Figure 6. Summed intensities of mass 29 ion sequence (points) and mass 27 ion sequence (open circles) as a function of pressure in the photoionization of ethylene at 923Å.

around the origin of the plot. On the other hand, it may be recalled that signals due to this ion sequence, albeit small, were also detected in the 1087Å photoionization of ethylene. Hence, it is reasonable to assume that the $C_2H_5^+$ ion and the follow-on ion sequence is due to the process

$$C_2H_4^+ + C_2H_4 \rightarrow C_2H_5^+ + C_2H_3 \qquad (15)$$

The clearer observation of $C_2H_5^+$ and its reaction sequence at a wavelength of 923Å compared with 1087Å, is mainly due to the higher intensity available with the light source combined with a 3 times higher ionization cross section of ethylene at 923Å. An additional factor may be the participation of excited ethylene ions, which according to a mass spectrometric study of Botter, et al[27] can be formed at wavelengths below about 1010Å. At 923Å as much as 2/3 of the total ions produced by photoionization may be in an excited state. The quantitative evaluation of the data shows that the ethylene parent ion reactions (7) and (15) have the following probabilities: 83 percent produce $C_2H_5^+$; 11 percent produce $C_4H_7^+$; and 6 percent produce $C_2H_5^+$. The product channel ratio for reaction (7) determined in this case is in reasonable agreement with that found for the same reaction in the 1087Å photoionization of ethylene. Any difference beyond the experimental error must be attributed to the participation of excited ethylene ions.

The formation of butene ions $C_4H_8^+$ via reaction (9) is shown in Figure 4 in comparison to that determined at 1087Å. As in that case, a linear pressure dependence is observed for the intensity ratio at M56 to that of all other $C_2H_6^+$ product ions. However, the rate of M56 formation is only about half that observed at 1087Å. Again, this behavior is indicative

of excited ethylene ions. Due to the additional energy content, the $C_4H_8^+$ collision complex would have a shorter lifetime, so that its stabilization by third body collision is less efficient.

The origin of the M27 may now be discussed. This ion is not believed to be formed from $C_2H_6^+$ in a manner similar to M29, because there is no evidence for M27 or the follow-on ions 40 and 54 in the photoionization of ethylene at 1087Å. However, in a mixture of acetylene and ethylene at the same wavelength very weak signals were observed at the corresponding mass numbers, indicating the reaction

$$C_2H_2^+ + C_2H_4 \rightarrow C_2H_3^+ + C_2H_3 \qquad (16)$$

Since the ionizing energy at 923Å lies only 0.3 eV above the threshold of $C_2H_2^+$ formation from ethylene, the acetylene ion cannot carry much internal energy and should behave similar to that formed from acetylene at 1087Å. However, at 923Å the formation of $C_2H_3^+$ according to reaction (16) would be more pronounced due to the higher ion intensity, and because of the absence of acetylene which diverts a considerable portion of acetylene ions to the M50 and M51 products due to reaction (4). Figure 6 shows also a plot of the sum of M27 and follow-on ion intensity versus pressure. The behavior is similar to that of the sum of M29 and follow-on ions, i.e. the pressure dependence is more linear, than one would expect for a secondary ion sequence. It should be noted that in the case of the $C_2H_3^+$ ion (but not for the $C_2H_5^+$ ion), there may be a small contribution to its intensity from the dissociative photoionization of ethylene. The

threshold for $C_2H_3^+$ formation by that process lies at 898Å, i.e. 25Å toward lower wavelengths. While the applied spectral resolution excludes the direct admission of this radiation to the ion chamber, radiation of shorter wavelengths may nevertheless be present as scattered light.

The $C_2H_3^+$ ion sequence constitutes about 2 percent of the total ion intensity, and about 20 percent of the acetylene ion intensity if it is counted fully as being due to reaction (16). The ratio of acetylene to ethylene ions thus produced by photoionization is $R = (C_2H_2^+)_o/(C_2H_6^+)_o$ = 0.14, if the M27 sequence is added to that of M26, and R = 0.12 if it is not. These ratios are smaller than those found in other studies of the photoionization of ethylene at 923Å, but they are still within the same order of magnitude. From the data of Botter, et al.[27] one obtains R = 0.21, the data of Brehm[28] yield R = 0.16 and those of Schoen[29] R = 0.20. A portion of the discrepancy may be due to the varying efficiencies of the electron multiplier detectors used in these studies. From electron impact ionization studies of ion reactions in ethylene it has been concluded[26] that charge transfer of $C_2H_2^+$ to ethylene produces some losses of acetylene ions. Since the data obtained for acetylene-ethylene mixtures at 1087Å gave no evidence for charge transfer, and the probability for this process was shown to be less than 15 percent of the total reaction probability, the effect of charge transfer to the $(C_2H_2^+)_o/(C_2H_6^+)_o$ ratio must be slight.

If the reactions assigned to the acetylene ions are reactions (10) and (16), the branching ratio found for reaction (10) from the photoionization of ethylene at 923Å is $C_3H_3^+/C_4H_5^+ = 2.1$. This agrees within

experimental error with the ratio found for the same reaction in a mixture of acetylene and ethylene, $C_3H_3^+/C_4H_3^+ = 2.4$, when the photoionizing wavelength was 1087Å. Because of the contribution of a dissociative photoionization process to the M27 ion sequence when ethylene is photoionized at 1087Å, the efficiency of reaction (16) can only to estimated. If half of the M27 sequence ion intensity is due to reaction (16), its rate is ten percent of the rate reaction (10), i.e. about 14 percent of the $C_2H_2^+$ ions reacting with ethylene yield $C_2H_3^+$.

Having assigned the various products to reactions of either ethylene or acetylene ions reacting with ethylene, the associated reaction rate coefficients can be determined from the decrease of the M28 and M26 ion intensities when compared to the total ion intensities in the corresponding ion sequences. The absolute values of the rate constants thus determined are $k_{4+12} = 0.88 \times 10^{-9}$ cc/molecule sec., and $k_{7+13} = 1.31 \times 10^{-9}$ cc/molecule sec. The former value constitutes only 70 percent of the rates coefficient for ethylene ions formed at 1087Å. This behavior is presumably associated with excited ethylene ions formed at 923Å. The latter rate coefficient is in excellent agreement with the value found for acetylene ions formed at 1087Å, and thus indicates that, in accord with expectation, the $C_2H_2^+$ ion formed from ethylene at 923Å is essentially identical with that formed at 1087Å by the photoionization of acetylene.

Further data have been obtained for reactions of acetylene and ethylene ions with methane, and for some reactions involving methane ions. These results have not been evaluated and will be discussed in future reports.

B. THEORETICAL STUDIES

During the current quarterly reporting period the major theoretical effort has been directed in two areas: (1) an investigation on the electron impact excitation of the dayglow, and (2) a reassessment on the presence of carbon atoms in the upper atmosphere of Venus.

In each case the subject matter of these investigations has been submitted for publication in scientific journals. Specifically the two papers submitted are "Electron Impact Excitation of the Dayglow," by A. Dalgarno, M. B. McElroy and A. E. Stewart, Journal of Atmospheric Sciences, 26, #4, 753 (1969), and "Carbon Atoms in the Upper Atmosphere of Venus," by F. F. Marmo and A. Engelman, accepted for publication in ICARUS. The results of these investigations are briefly discussed below.

(1) Electron Impact Excitation of the Dayglow

Calculations are described of the equilibrium velocity distributions of the photoelectrons produced in the "F" region by solar ionizing radiation. Detailed estimates are presented of the intensities and altitude profiles of emission features of atomic oxygen, molecular nitrogen, and molecular oxygen, appearing in the dayglow as a result of photoelectron impacts.

The fast photoelectrons, produced in the upper atmosphere by the absorption of solar ultraviolet radiation in ionizing transitions, lose energy in collision processes leading to ionization and excitation of the neutral particles and to heating of the electron and ion gases. The

excitation processes produce a substantial component of the dayglow luminosity of the upper atmosphere, the observation and interpretation of which can provide detailed information on the distribution of energy sources in the daytime atmosphere. The prediction of the intensities of the dayglow emission features is similar to the calculation of electron heating rates,[30,31] but involves a more detailed description of the individual processes that slow down the photoelectrons and a more precise calculation of the apportionment of the available energy among them.

The calculation of the initial energy spectrum of the photoelectrons, which involves a choice of model atmospheres, of absorption and photoionization cross sections, and of solar ultraviolet intensities, has been described in detail.[30,31] The predicted initial spectra at various altitudes for a solar zenith angle of 72 degrees and a model atmosphere with an exospheric temperature of 750°K are shown in Figure 7.

The photoelectrons lose energy by exciting and ionizing the neutral particle constituents of the atmosphere and by elastic collisions with the ambient electrons.[30] Many processes contribute to the energy degradation but few of the cross sections are known with precision.

For atomic oxygen, the ionization cross section has been measured by Fite and Brackmann[32] and Rothe, et al.[33] the cross sections for populating the upper levels of the green and red lines.

$$e + O\ (^3P) \rightarrow e + O\ (^1S) \qquad (17)$$

$$e + O\ (^3P) \rightarrow e + O\ (^1D) \qquad (18)$$

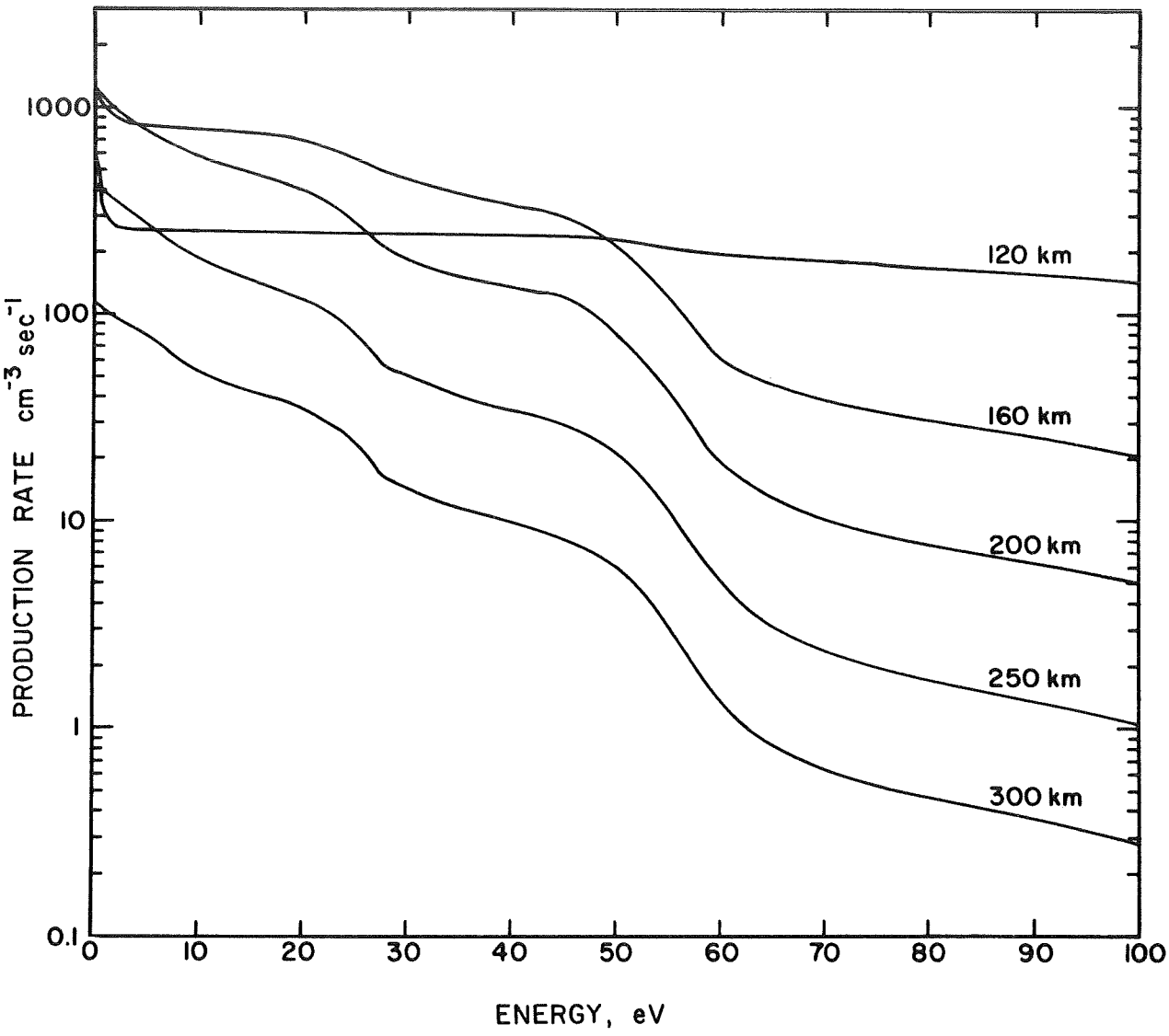

Fig. 7. Production rate of photoelectrons with initial energy greater than E as a function of E for various altitudes.

have been calculated by Smith, et al.[34] and the cross section for populating the 3s ^3S state has been calculated by Stauffer and McDowell.[35]

For molecular oxygen, the ionization cross section has been measured by Tate and Smith,[36] Craggs, et al,[37] Lampe, et al,[38] Fite and Brackman,[32] Rapp and Englander-Golden,[39] Schram, et al,[40] and Schram, et al.[41] The cross section for simultaneous ionization into the b $^4\Sigma_g^-$ state of O_2^+ has been measured by Stewart and Gabathuler,[42] Nishimura,[43,44] and Aarts and de Heer.[45] The cross section for dissociative attachment has been measured by Rapp and Briglia,[46] and some cross-section data for the inelastic scattering of electrons with energies between 4.5 eV and 12.5 eV have been obtained by Schulz and Dowell[47] (see also McGowan, et al.[48]). Recently, Hake and Phelps[49] have analyzed energy loss in O_2 to derive a set of inelastic cross sections with thresholds at 4.4 eV, 5.0 eV, 8.0 eV, and 9.7 eV. The inelastic scattering of electrons at energies in the region of 500 eV has been investigated for O_2 by Lassettre, et al.[50] and Silverman and Lassettre.[51] Suitably analyzed, they can yield the Born approximation to the cross section at other impact energies, and the Born approximation for the dissociation of O_2 in the Schumann-Runge continuum has been so derived by Silverman and Lassettre.[51]

The ionization cross section for N_2 has been measured by Tate and Smith,[35] Lampe, et al,[38] Peterson,[52] Rapp and Englander-Golden,[39] and Schram, et al.[40,41] The excitation function for the production of the first negative system has been measured by Stewart,[53] Sheridan, et al,[54]

Hayakawa and Nishimura,[55] Davidson and O'Neil,[56] McConkey and Latimer,[57] McConkey, et al,[58] Holland,[59] Srivastava and Mirza,[60] Nishimura[44] and Aarts, et al.[61] The excitation functions for populating the C $^3\Pi_u$ state of N_2, the upper level of the second positive system, are also available (Thieme,[62] Langstroth,[63] Herrmann,[64] Stewart and Gabathuler,[42] Kishko and Kuchinka,[65] Zapesochnyi and Kishko,[66] Fink and Welge,[67] Zapesochnyi and Skubenich,[68] Jobe, et al,[69] Burns, et al.[70]), as are those for simultaneous excitation and ionization to the $A^2\Pi_g$ state of N_2, the upper level of the first positive band system (Williams,[71] Zapesochnyi and Skubenich[68]), and for populating the a $^1\Pi_g$ state, the upper level of the Lyman-Birge-Hopfield band system.[72] Cross sections for the electron impact dissociation of N_2 have been measured by Winters.[73] Engelhardt, et al[74] have obtained an estimate of the cross section for a transition occurring near 6.7 eV, which probably corresponds to excitations of the B $^3\Pi_g$ and A $^3\Sigma_u^+$ states.[75] The cross sections measured by Zapesochnyi and Skubenich[68] for the excitation of the B $^3\Pi_g$ state are large, and we shall assume that direct excitation to the A $^3\Sigma_u^+$ state is negligible compared with cascading from the B $^3\Pi_g$ state. The A $^3\Sigma_u^+$ state, which is the upper level of the Vegard-Kaplan band system, is the lowest lying excited electronic state of N_2. Its threshold occurs at 6.5 eV.[76]

The inelastic scattering of electrons with energies in the region of 500 eV has been investigated by Lassettre and Krasnow,[77] Silverman and Lassettre,[78] Geiger and Stickel,[79] Lassettre, et al,[80] and Meyer and Lassettre;[81] and Takayanagi and Takahashi[75] have derived from the high-velocity data the Born approximation to the cross sections for excitation of the a $^1\Pi_g$ state, the b $^1\Pi_u$ state, and a group of states of N_2

near 14 eV. The a $^1\Pi_g$ state is the upper level of the Lyman-Birge-Hopfield band system, and the b $^1\Pi_u$ state is the upper level of the Birge-Hopfield and Janin systems.

Below 6.5 eV, the photoelectrons lose energy through excitation of the vibrational levels of N_2, a process that has been studied experimentally by Haas,[82] Schulz,[83-85] Schulz and Koons,[86] Boness and Hasted,[87] and Andrick and Ehrhardt.[88] The experimental data are satisfactorily reproduced by the model calculations of Chen.[89]

We have supplemented the experimental data by the use of some simple rules relating cross sections for transitions of similar kinds. Thus, we assume for optically allowed transitions that the cross sections have the same shape as a function of E/W, where E is the electron energy and W is the threshold energy, as that measured for the 1s-2p transition of atomic hydrogen[90,91] and to have magnitudes Q_{max} given by

$$\frac{W^2 Q_{max}}{f} = 2.1 \times 10^{-14} \text{ eV}^2 \text{ cm}^2 \qquad (19)$$

where f is the optical oscillator strength of the transition. For strong atomic transitions, the cross sections will usually be accurate to within a factor of two.[92] For the cross sections of transitions involving a change in spin multiplicity, we adopted for the appropriate shape as a function of E/W that for the $1\ ^1S\text{-}2\ ^3S$ transition in helium[93] and we assumed that the magnitudes are given by

$$W^2\ Q_{max} = 1.5 \times 10^{-15} \text{ eV}^2 \text{ cm}^2. \qquad (20)$$

For forbidden transitions not involving a change in spin multiplicity, we assumed that the cross sections have the same shape as a function of E/W as that measured for the 1s-2s transition in atomic hydrogen[94] and we assumed (20) for the magnitudes.

Some check on the optically allowed transitions is provided by the requirement that at high electron energies the energy loss rate be given by the Bethe formula

$$\frac{dE}{dx} = \frac{-1.9 \times 10^{-12}}{E} \sum_i n_i \ell n\ (E/I_i)\ \text{eV cm}^{-1} \qquad (21)$$

where n_i is the number density of the constituent i, and I_i is its mean excitation energy, which takes the values of 15.0 eV for atomic hydrogen, 42.3 eV for helium, 82 eV for nitrogen, and 94 eV for atomic and molecular oxygen.

There are no measurements for the atmospheric gases of the distribution of secondary electrons produced by ionization by the primary photoelectrons, but approximate theoretical values can be obtained from optical photoionization data by use of the Bethe dipole approximation.[75,95] The slow secondaries lose most of their energy in the excitation of the vibrational levels of molecular nitrogen and in elastic collisions with the ambient electron gas so that a gross representation of their distribution suffices for the prediction of most of the dayglow emission features. We assume that electrons with energies greater than 68 eV produce on ion-pair for every 34 eV of energy, that those with energies between 68 eV and 25 eV produce one ion-pair, and that the secondary electrons after completion of the ionizing events have a Maxwellian velocity distribution characterized by a temperature equivalent to a mean energy of 5 eV.

Secondary electrons are also produced by the radiative emission of ultraviolet photons from excited states, populated by photoionization and by electron impact. These sources can be included straightforwardly.

Although the accuracy of the cross sections adopted for any specific collision process may not be high, the collection of cross-section data should describe adequately the overall efficiency of energy loss as a function of energy and yield a satisfactory representation of the equilibrium velocity distribution of the photoelectrons.

The energy loss functions or stopping cross sections,

$$L\ (E|i) = \frac{1}{n_i}\ \frac{dE(i)}{dx}\ \text{eV cm}^2 \qquad (22)$$

are illustrated in Figure 8 for molecular nitrogen, molecular oxygen, atomic oxygen, and helium, the helium values being based on the measurements of Smith,[96] Maier-Leibnitz,[97] and Schulz and Fox.[93] The loss functions for N_2 and O_2 are about a factor of two larger than those computed by Green and Barth,[98] and the loss function for O is about 50 percent larger. Green and Barth do not include helium as a constituent. The differences afford a measure of the uncertainties in the calculation of energy loss rates.

An energy loss function for the atmosphere at any given altitude can be defined by

$$L(E) = \frac{\sum_i n_i\ L(E/i)}{\sum_i n_i}\ \text{eV cm}^2, \qquad (23)$$

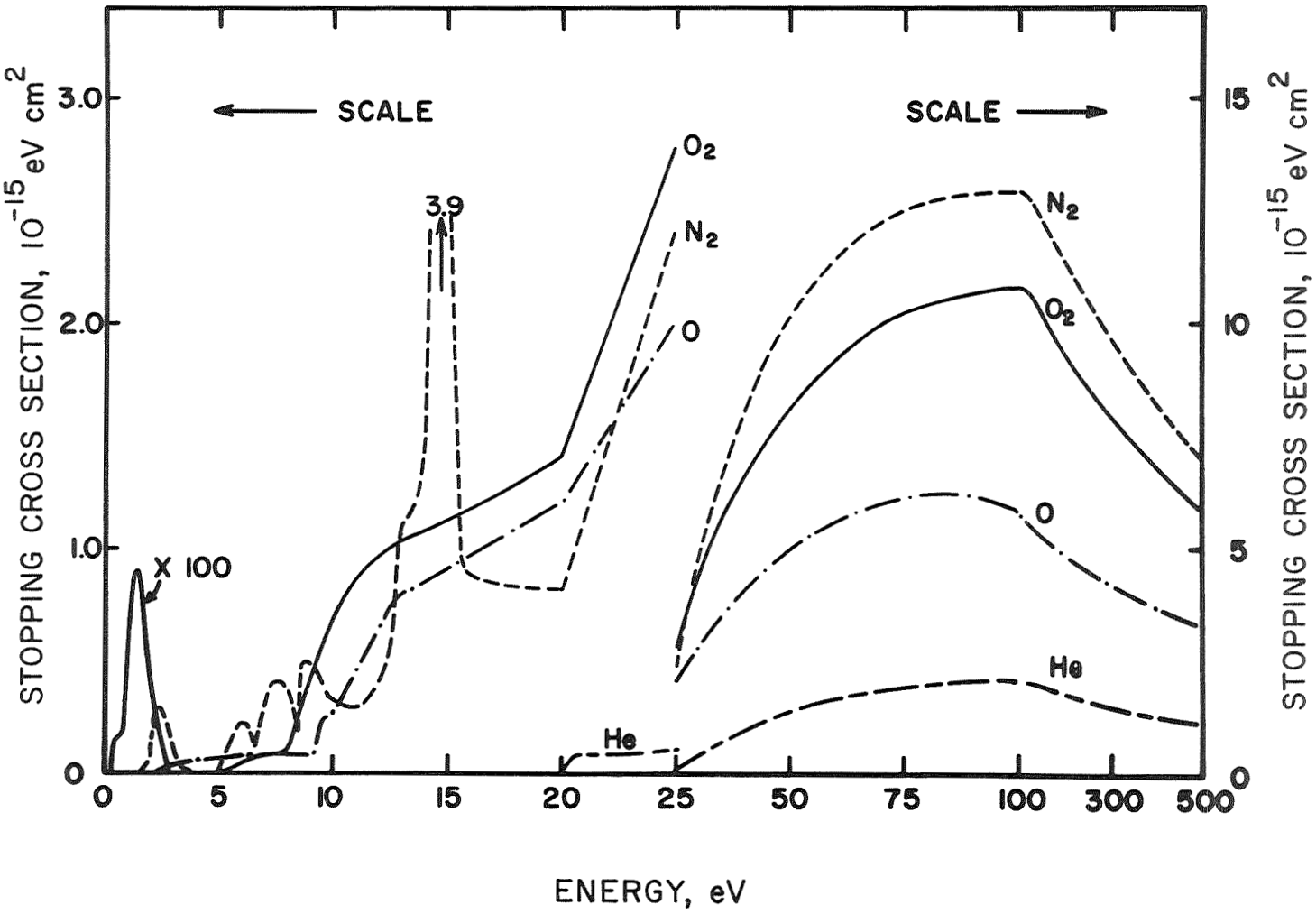

Fig. 8. Stopping cross sections or loss functions for O, O_2, N_2, and He. Note the two vertical scales and the changes in the horizontal scale at 25 eV and at 100 eV.

the summation including the contribution to energy loss arising from elastic collisions with the thermal electron gas. The quantity L (E) varies slowly with altitude except at energies below about 20 eV, as is clear from the similar shapes at energies above 20 eV of the individual loss functions.

Suppose there are f(E)dE photoelectrons per unit volume with energies lying between E and E + dE. Then in equilibrium the rate at which the photoelectrons leave the energy interval E, E + dE equals the rate at which they enter. It follows that if p_j is the rate of production of electrons of energy E_j and we assume that energy loss is a continuous function of E,

$$f(E) = \frac{\sum_{E_j > E} p_j}{v \sum_i n_i \, L(E)} \quad eV^{-1} \, cm^{-3}, \tag{24}$$

where v is the electron velocity corresponding to an energy E. The assumption of continuous energy loss becomes inadequate at low energies. Recent calculations by Stewart[99] suggest that dayglow intensities predicted on the basis of continuous energy loss may be too high by a factor of up to two, if the process leading to the emission has a threshold energy of only a few eV.

Formula 24 also assumed that the photoelectrons are absorbed locally. The assumption is satisfactory at altitudes below 250 km, where most of the dayglow emissions occur, but it leads to overestimates of the intensities at higher altitudes.

The calculated equilibrium photoelectron fluxes vf(E) of the photoelectrons are illustrated in Figure 9 as a function of energy at various altitudes. They are qualitatively similar to the results of some less detailed calculations by Hoegy, et al.[100] The minimum, occurring near 2.5 eV at low altitudes, reflects the efficiency of vibrational excitation of N_2. The minimum is followed by a broader maximum between 3.5 eV and 5 eV where the energy loss is mainly due to the excitation of metastable states of oxygen. At altitudes above 200 km, elastic collisions with the ambient electrons are the dominant energy-loss mechanism at low energies and the low-energy structure disappears.

If $\sigma_i(E|m)$ is the cross section for exciting level m of constituent i, the rate of population of level m by electron impact, $q(i|m)$, is given by

$$q(i|m) = n_i \int f(E)\ v\ \sigma_i(E|m)\ dE\ cm^{-3}\ sec^{-1} \qquad (25)$$

To (25) must be added contributions from secondary electrons and from cascading from higher levels.

The inclusion of energy losses to ambient electrons in the expression (23) for the loss function affects the altitude dependence of $q(i|m)$ above about 225 km. At high altitudes the photoelectrons are produced mainly from atomic oxygen and lose their energy to atomic oxygen and the electron gas. If their energy is greater than the critical energy E_c, above which the most efficient cooling process is inelastic collisions with atomic oxygen and below which it is elastic collisions with ambient electrons[101] the velocity distribution f(E) varies only slowly with altitude since both the numerator and the denominator in Equation (24) vary as the atomic-

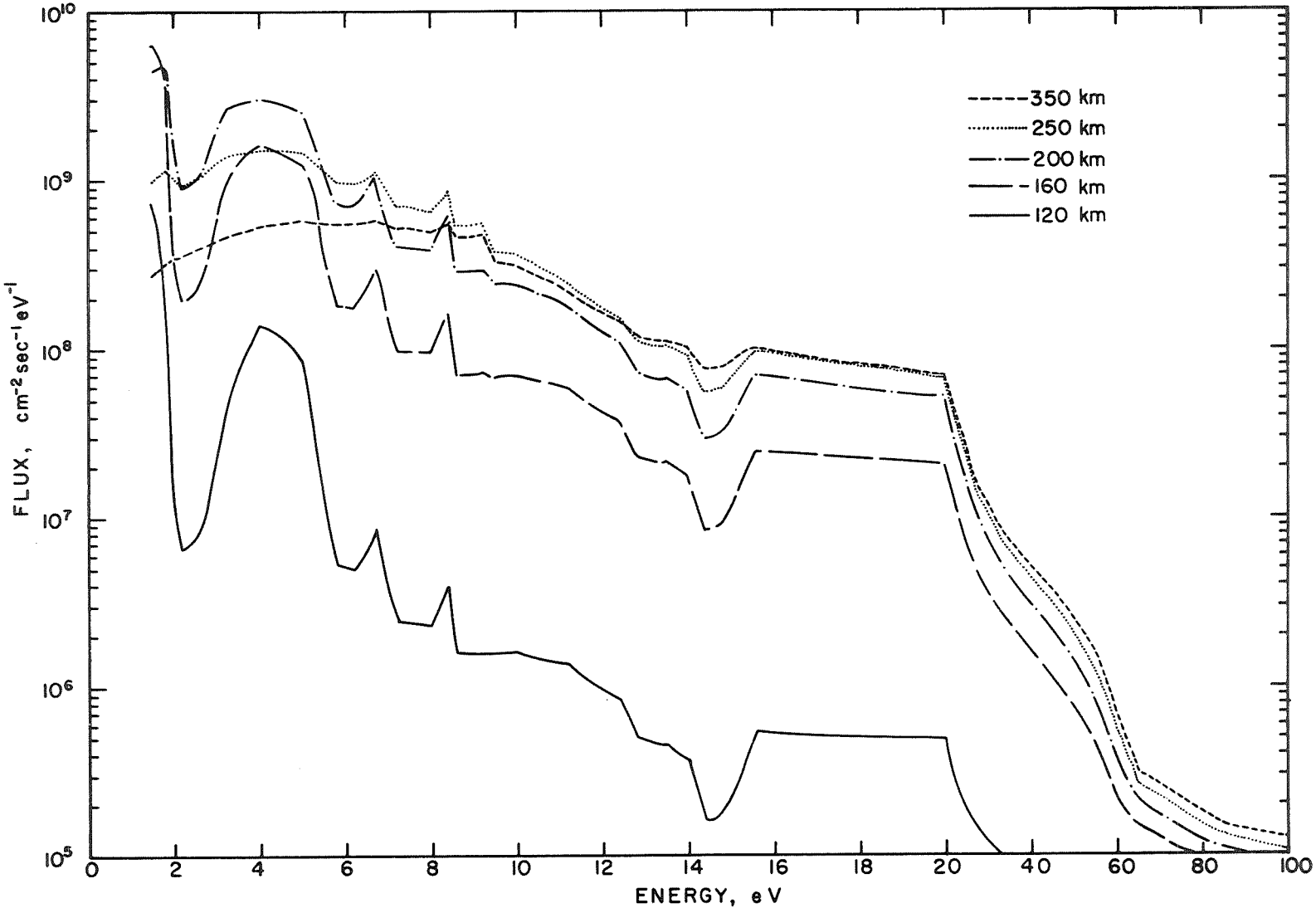

Fig. 9. Equilibrium photoelectron fluxes vf(E) as a function of energy at various altitudes. Note the change in the horizontal scale at 20 eV.

oxygen density; if their energy is less than E_c, f(E) varies as $n(O)/n_e$, since in this case, the denominator varies as the electron density. Hence, if the major contribution to q (i|m) comes from photoelectrons with energies greater than E_c, q (i|m) will be roughly proportional to n_i; while if it comes from energies less than E_c, q(i|m) will be roughly proportional to n_i $n(O)/n_e$. The deviation from proportionality to n_i is most noticeable for low-lying and metastable states, as can be seen from Figures 10, 13, and 14.

Atomic Oxygen λ 1302-1306Å. The resonance triplet of atomic oxygen,

$$O\ (2p^3\ 3s\ ^3S^o) \rightarrow O\ (2p^4\ ^3P) + h\nu$$

consists of three lines at 1302, 1304, and 1306Å. We find that for a solar angle of 72 degrees, the rate of population of the $^3S^o$ level by photoelectrons reaches a maximum of 250 cm^{-3} sec^{-1} at an altitude of 175 km. The detailed profile is presented in Figure 10. The total zenith production rate above 120 km is 2.8×10^9 cm^{-2} sec^{-1}. The values are comparable to those obtained for an overhead sun by Thomatsu[102] and Green and Barth.[98]

The 1304Å triplet has been observed in the dayglow.[103-109] Theoretical interpretations of the altitude profiles, based upon resonant scattering of sunlight, appeared to demand an additional source of radiation near 200 km.[102,104,110] There are several uncertainties in the original interpretation and the position remains obscure.[111-113] However, it is clear that photoelectron impact is a major additional source that must be included in the theoretical analysis.

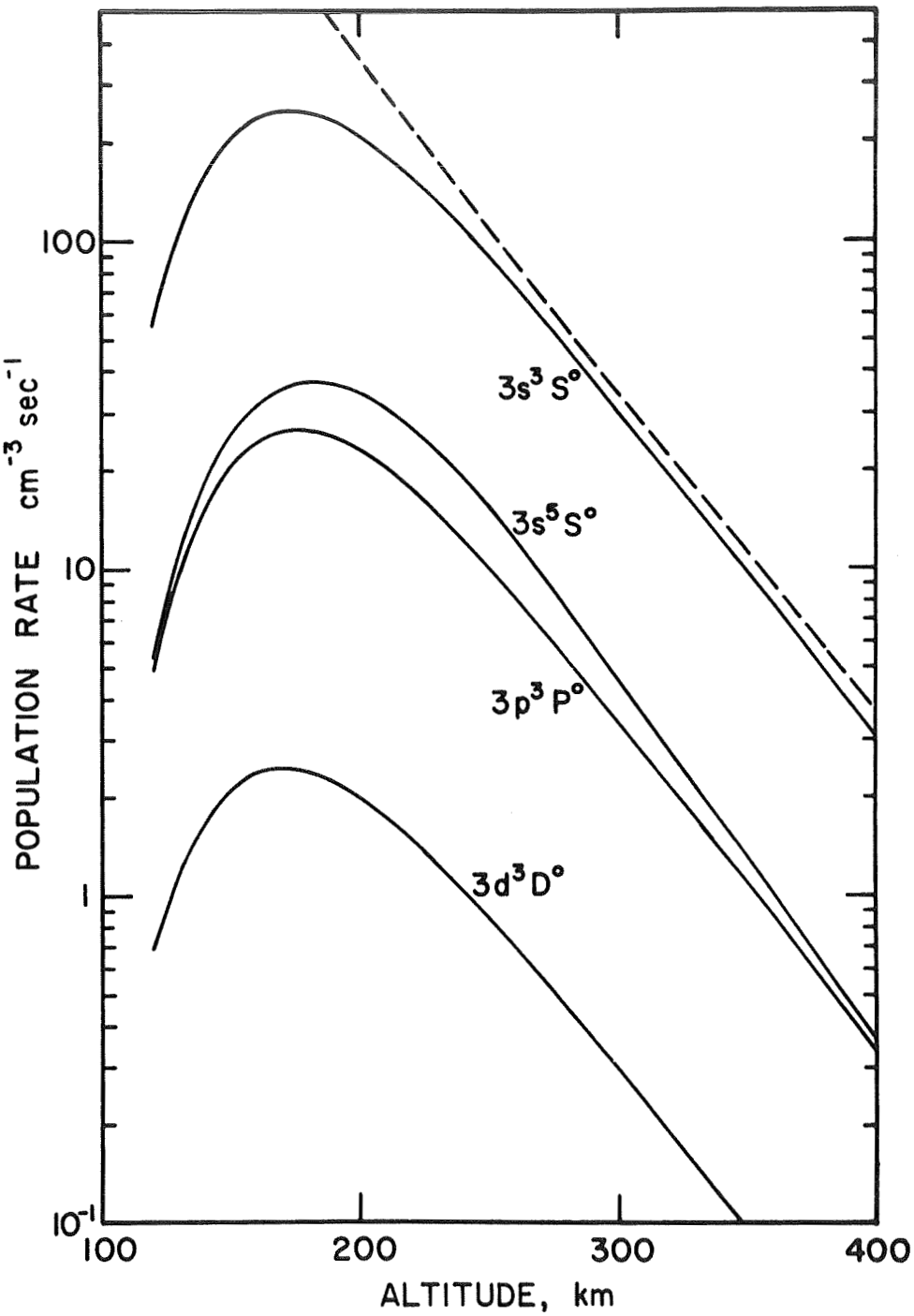

Fig. 10 Rates of population of excited states of atomic oxygen as functions of altitude. The dashed line is proportional to the atomic-oxygen density.

Atomic oxygen λ 1356Å. Donahue and Fastie[104] and Fastie, et al.[106] have observed a dayglow feature at 1356Å, which they identify as a forbidden line of atomic oxygen arising from the transition

$$O\ (2p^3\ 3s\ {}^5S^o) \rightarrow O\ (2p^4\ {}^3P) + h\nu.$$

Donahue[112] concluded that a local excitation source must be invoked, and photoelectron impact is an obvious possibility.[102,110] The predicted excitation rate is shown in Figure 10.

The $(2p^3\ 3s)^5S^o_2$ level decays by spontaneous emission to the ground ^3P state producing a photon at 1356Å, and to the metastable ^1D state producing a photon at 1728Å. The radiative probability for the $^3P_1$-$^5S_2$ transition is 390 sec^{-1}, for the $^3P_2$-$^5S_2$ it is 1300 sec^{-1}, and for the $^1D_2$-$^5S_2$ it is 2 sec^{-1}.[114] Deactivation is unlikely to affect the emission of 1356Å and the emission rate of 1356Å photons will be effectively identical to the production rate in Figure 10.

The observed flux is affected by absorption by molecular oxygen. Figure 11 illustrates the overhead flux as a function of altitude, with and without the inclusion of molecular oxygen absorption, and on the assumption that the atmosphere is optically thin to resonance absorption by atomic oxygen. The optical depth reaches unity at an altitude of about 120 km so that there is some uncertainty in the predicted emission profile at the lowest altitudes. The observational data, included in Figure 11 are in substantial agreement with the theoretical predictions. The 3-0 Lyman-Birge-Hopfield band of N_2 is located in the region of 1354Å, and it is included in the observations. Our calculations indicate that it contributes 5 percent of the observed intensity.

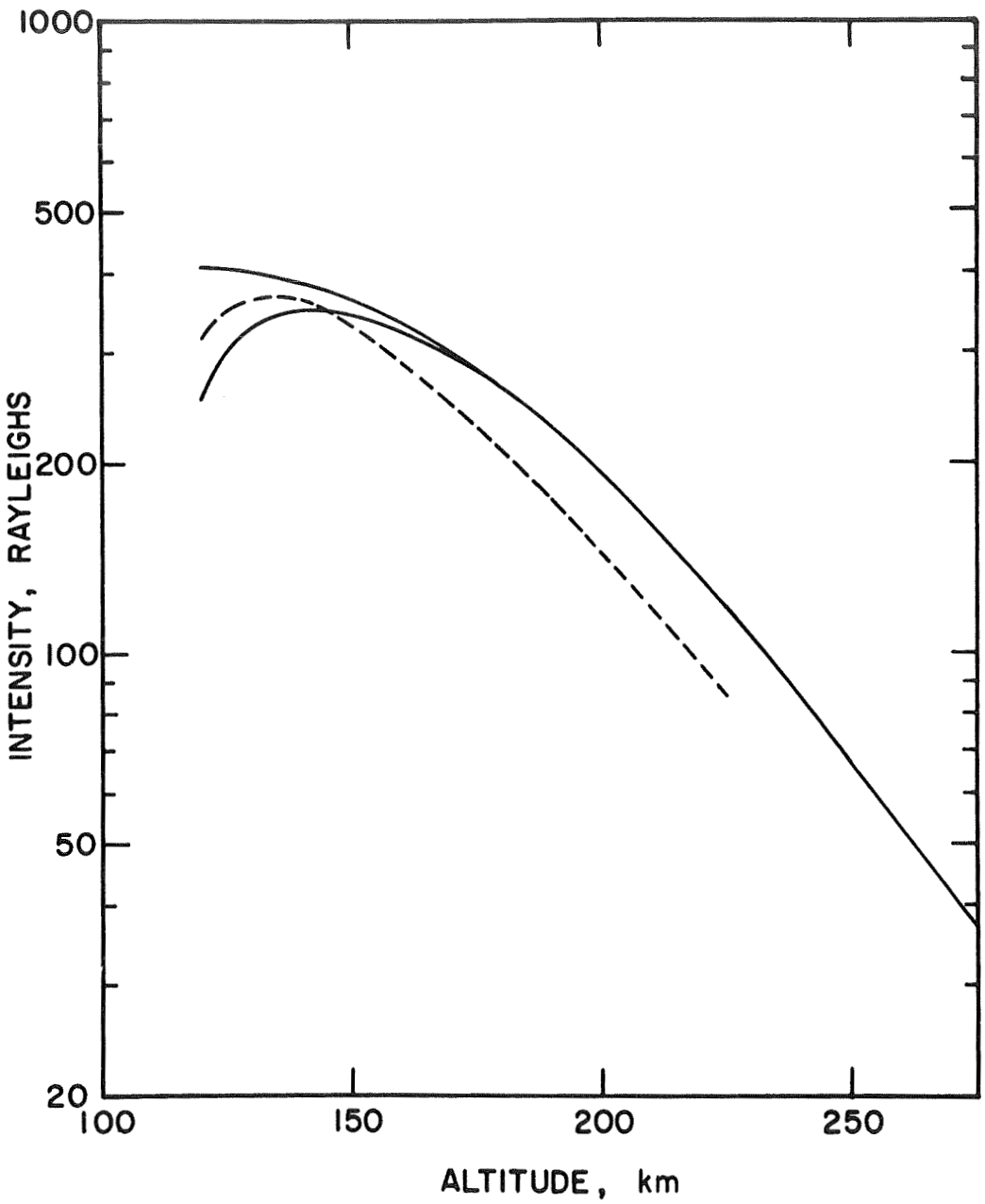

Fig.11 . Overhead intensity of the λ 1356 emission of atomic oxygen as a function of altitude. The upper branch of the solid curve represents the intensity in the absence of absorption by molecular oxygen, and the lower branch the intensity with this absorption included. The dashed curve is the observational data of Fastie et al. (Ref. 106)

Green and Barth[98] predicted a much greater intensity, owing to the adoption of a cross section for the excitation process that remains large over an extended energy range.

Atomic oxygen λ 8446Å. The $(2p^3 3p)^3P$ state of atomic oxygen decays by an allowed transition to the $(2p^3 3s)^3S^o$ state, emitting a photon at 8446Å. It is a familiar feature of auroral spectra. The predicted altitude profile is illustrated in Figure 10 and the overhead intensity flux in Figure 12.

The dayglow emission will be augmented by fluorescence of solar Lyman β, which can be absorbed by atomic oxygen into the $(2p^3 3d^3D)$ state. The ^3D state then radiates a photon at 11,340Å in a transition terminating at the upper level of the 8446Å line. The mechanism has been examined quantitatively by Shklovskii[115] and Brandt.[116] Adopting a Lyman β flux of 2×10^9 photons cm^{-2} sec^{-1},[117] and appropriately modifying Brandt's arguments, it appears that only 50 Rayleighs of 8446Å radiation will arise from the Lyman β source.

Atomic oxygen λ 7774Å. The infrared line of atomic oxygen at 7774Å arising from the $(2p^3 3p^5P)$ - $(2p^3 3s^5S)$ transition is also a familiar feature of auroral spectra. With our assumptions about cross sections, the emission intensity of 7774Å is comparable with that of 8446Å and the altitude profiles are essentially identical.

Atomic oxygen λ 1026Å. Atomic oxygen has a resonance line at 1026Å arising from the $(2p^3 3d^3D^o)$ - $(2p^4\ ^3P)$ transition. The atmosphere is optically thick in 1026Å and a substantial contribution to the population

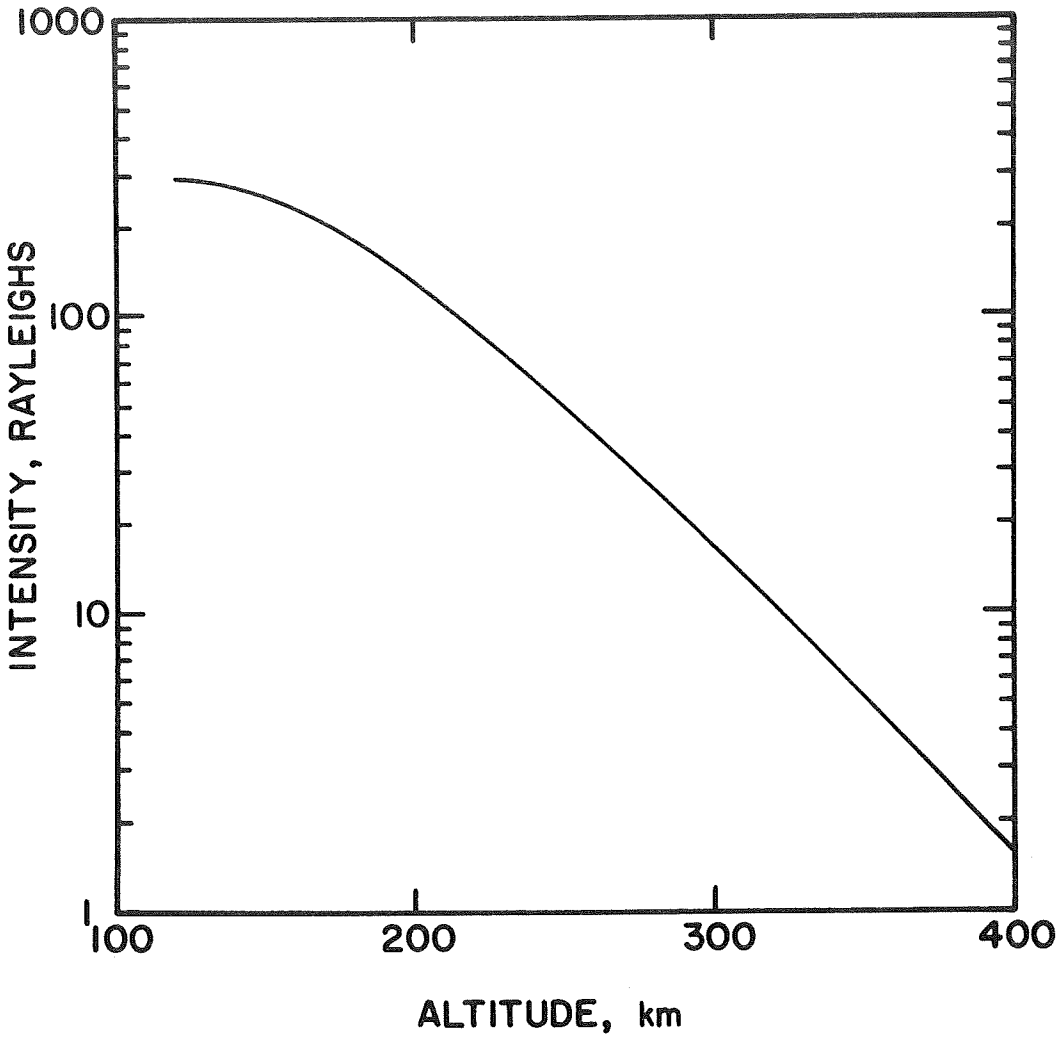

Fig. 12. Overhead intensity of the λ 8446 emission of atomic oxygen as a function of altitude.

of the upper level will result from resonant scattering. The rate of population of the $2p^3 3d\,^3D^o$ state by photoelectron impact is small. Its altitude profile is illustrated in Figure 10. The state can decay by radiating also at 11,340Å.

Other atomic oxygen ultraviolet lines. There are other lines of atomic oxygen that should appear in the ultraviolet dayglow. In particular, a line at 1152Å due to O ($2p^3 3s\,^1D^o$) - O ($2p^4\,^1D$) should be similar in profile to 1356Å but less intense, and a line at 989Å due to O ($2p^3 3s\,^3D^o$) - O ($2p^4\,^3P$) should be similar to 1304Å in profile but less intense. Estimates for an overhead sun have been given by Green and Barth.[98] The dayglow at 989Å will be modified by resonance scattering.

Atomic oxygen λ 5577Å. The photoelectron impact contribution to the population of the ^1S level of atomic oxygen is shown in Figure 13. Other excitation processes occur[118,119] but a detailed analysis of observational data carried out by Wallace and McElroy[120] established that photoelectron impact is a major source at high altitudes.

The ^1S level also decays by emitting photons at 2972Å and at 2958Å. The intensities will be 6 percent of that of the green line at 5577Å.

Atomic oxygen λ 6300Å. The photoelectron impact contribution to the population of the ^1D level of atomic oxygen is shown in Figure 13. The emission of the red line in the dayglow has been the subject of much discussion. Analysis by Noxon[121] and Dalgarno and Walker[122] showed that the ^1D level must undergo severe deactivation, and they argued that a

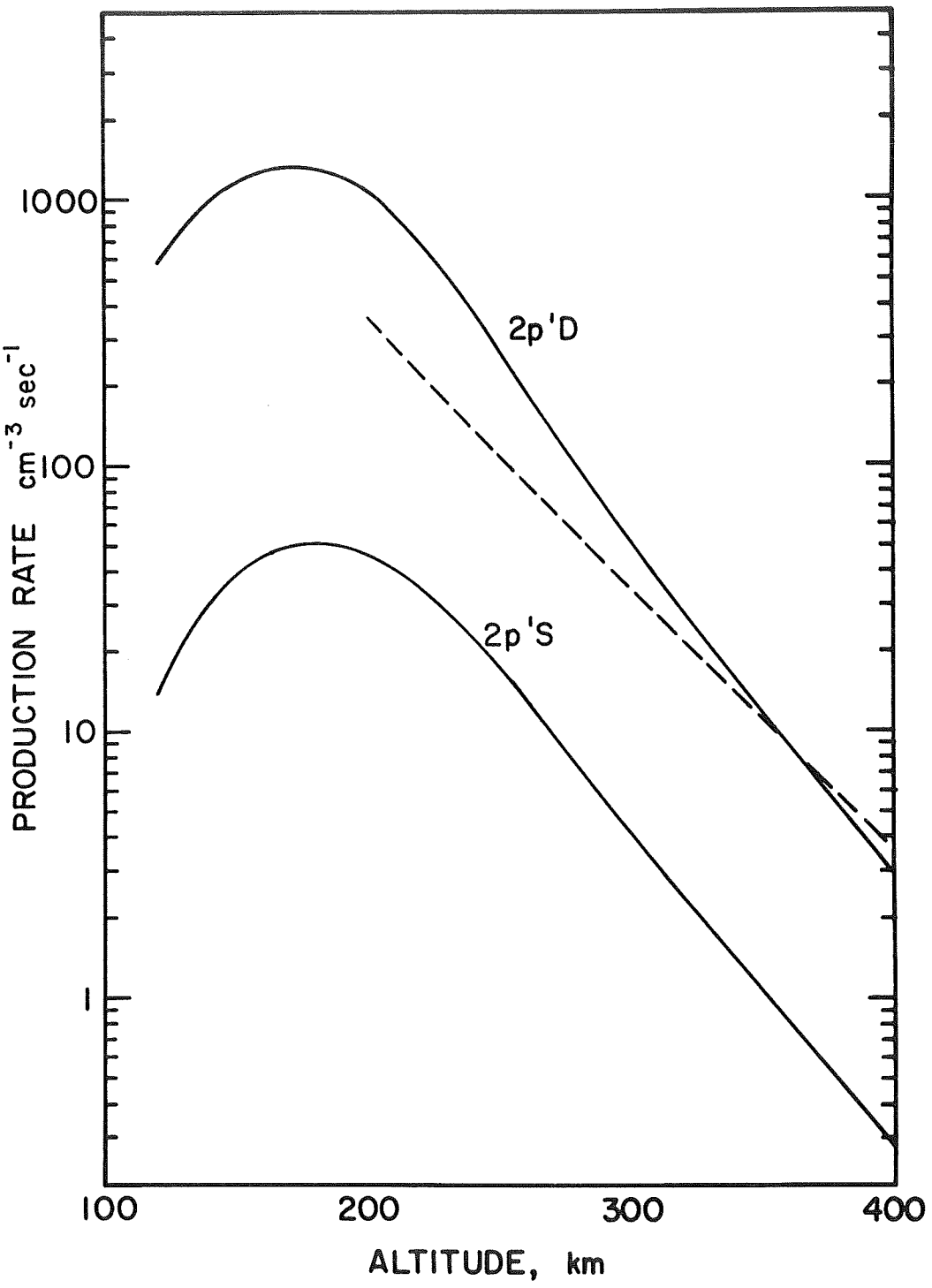

Fig. 13. Rates of population of the metastable ^{1}D and ^{1}S states of atomic oxygen as functions of altitude. The dashed line is proportional to the atomic-oxygen density.

high altitude source in addition to photodissociation and ionic recombination is required. The photoelectron contribution to the red-line emission has been calculated previously by Wallace and McElroy[120] and our results serve as a confirmation of their conclusions that photoelectron impact is indeed a major high altitude source. In most circumstances, the direct impact contribution by the energetic photoelectrons will be much larger than the contribution from thermal excitation by the heated electrons, and the enhancement of the red line by conjugate-point photoelectrons is produced directly by impact excitation rather than indirectly by heating of the ambient electron gas.

Dissociative excitation of O_2. The dissociative excitation of molecular oxygen by photon and electron impact, which are important low-altitude sources of O (^1D) atoms, may also be abundant low-altitude sources of more highly excited oxygen atoms. Reliable quantitative estimates are precluded by the lack of information on the cross sections.

First negative system of N_2^+. The production of N_2^+ molecules in the $B\ ^2\Sigma_u^+$ state by photoelectron impact with N_2 is shown in Figure 14. The production is small compared with that from resonance scattering of solar radiation by N_2^+ molecules at high altitudes.[120] At lower altitudes, where the equilibrium density of N_2^+ is small, the major source is probably simultaneous excitation and ionizationby solar radiation absorbed in a photoionizing transition.[30,123]

The infrared Meinel system of N_2^+. The production of N_2^+ molecules in the $A\ ^2\Pi_g$ state by photoelectron impact with N_2 is shown in Figure 14.

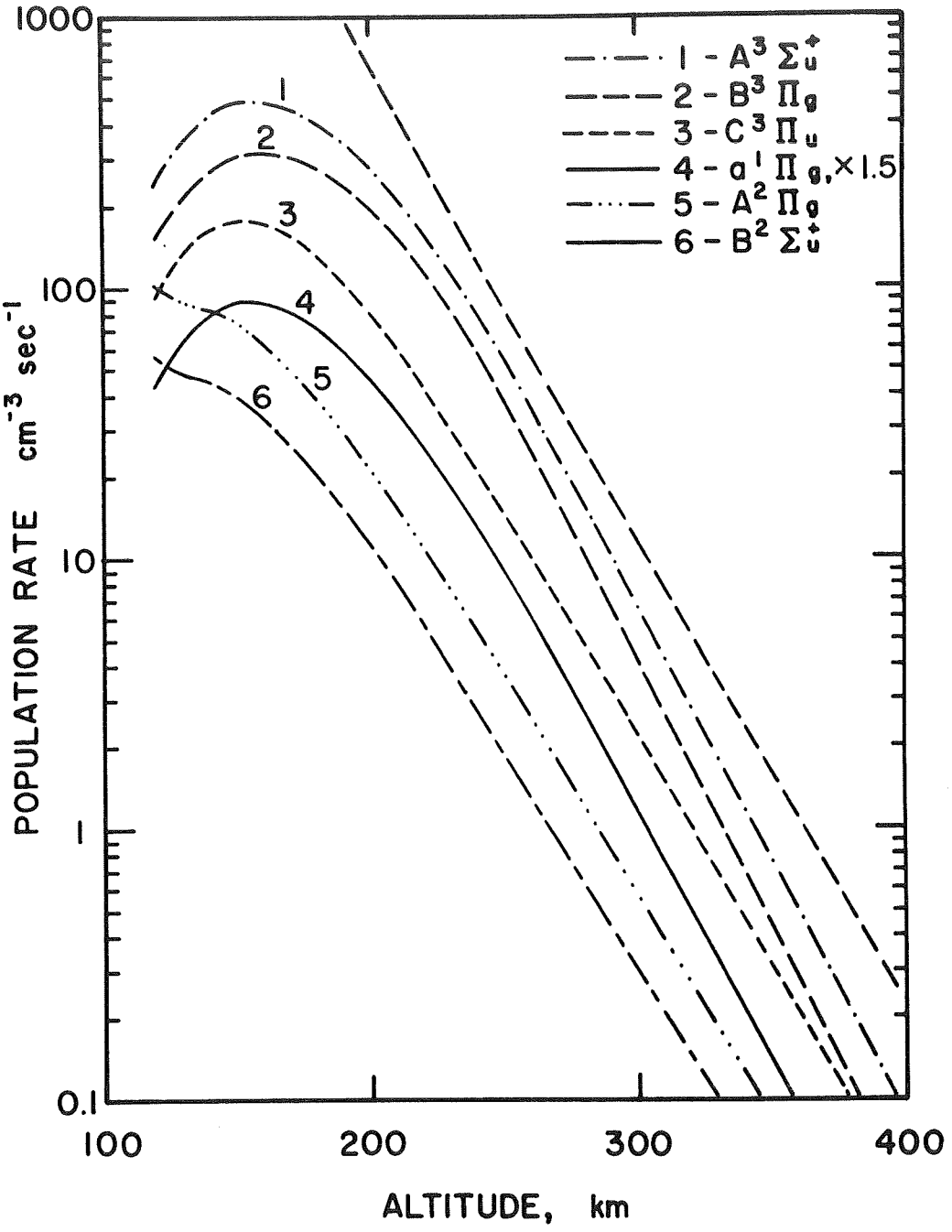

Fig. 14. Rates of population of excited states of N_2 (curves 1-4) and N_2^+ (curves 5 and 6) as functions of altitude. Curve 1, for the $A\ ^3\Sigma_u^+$ state, includes the contribution from cascade from higher states. The dashed line is proportional to the N_2 density.

The production rate has a value of 80 cm^{-3} sec^{-1} at 145 km. The luminosity profile and the vibrational distribution will be modified by resonant and fluorescent scattering of solar radiation by the ambient N_2^+ molecules, by simultaneous excitation and ionization of N_2 in photoionizing transitions, and possibly by ion-molecule reations.(123)

The second positive band system of N_2. The second positive band system of N_2 is of particular interest since photoelectron impact is the only significant source of N_2 ($C\ ^3\Pi_u$) molecules in the atmosphere and its emission profile is unaffected by deactivation processes.(124) The predicted rate of population is shown in Figure 14 and the overhead intensity in Figure 15. The results are comparable with those of an earlier, more approximate calculation by Nagy and Fournier.(125)

The predicted vibrational distribution, based upon the cross-section data of Jobe, et al.(69) is presented in Table 3, as is the theoretical distribution, based upon the Franck-Condon factors tabulated by Nicholls.(126) The calculated overhead intensity of the 0-0 band at 3371Å above 165 km is 200 Rayleighs, in fair accord with the measured value of 400 Rayleighs.(124)

The first positive band system of N_2. The first positive band system arises from the $B\ ^3\Pi_g - A\ ^3\Sigma_u^+$ transition in N_2. It is populated by direct impact and by cascading, its upper level being the lower level of the second positive system. The excitation functions of Zapesochnyi and Skubenich(68) include the cascading contributions, but they do not report the excitation functions for the individual vibrational levels.

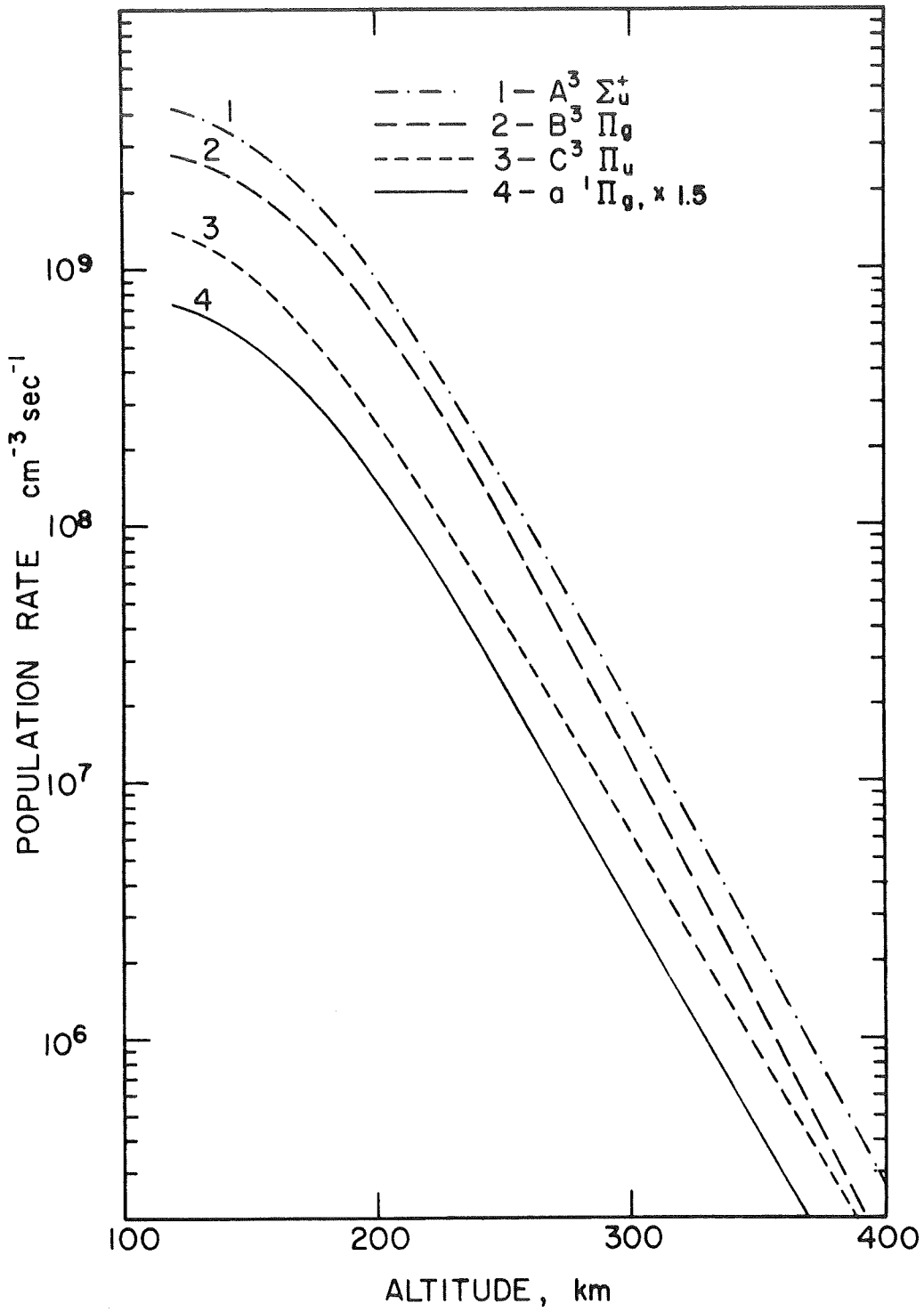

Fig. 15 Total rates of population of excited states of N_2 above a given altitude as functions of that altitude.

Table 3. Predicted vibrational distribution of the second positive-band system of N_2, expressed as a percentage of the total emission.

v′	v″	0	1	2	3	4	5	Σv″
0	a	28.5	17.4	6.5	1.9	0.5	0.1	54.9
	b	20.0	15.7	8.2	2.2	0.6	0.2	47.0
	c							55.0
1	a	15.9	6.5	5.9	4.9	2.3	0.8	30.8
	b	15.9	9.3	5.7	5.7	4.1	1.1	34.5
	c							27.0
2	a	2.1	4.4	0.4	0.6	1.3	1.0	10.5
	b	2.0	5.9	0.4	0.6	1.9	1.9	14.6
	c							14.0

a. Given by measurements of Jobe et al. (Ref. 69)

b. Computed from Franck-Condon factors (Ref. 126)

c. Computed from the absorption oscillator strengths of Ching et al. (Ref. 128)

The predicted rate of population is shown in Figure 14 and the overhead integrated rate of population in Figure 15. The profile may be significantly modified by resonance scattering of solar radiation by the metastable A $^3\Sigma_u^+$ state.[110]

The Vegard-Kaplan band system of N_2. The Vegard-Kaplan band system arises from the forbidden A $^3\Sigma_u^+$ - X $^1\Sigma_g^+$ transition in N_2. The major source of population is probably cascading in the first positive system. The rate of population is illustrated in Figures 14 and 15.

The emission profile is greatly modified by deactivation. Green and Barth[98] have investigated the effect, using electronic deactivation coefficients and transition probabilities listed by Hunten and McElroy.[127] Because of vibrational interchange processes

$$N_2(A\ ^3\Sigma_u^+,\ v) + N_2(X\ ^1\Sigma_g^+,\ v = 0) \rightarrow N_2(A\ ^3\Sigma_u^+,\ v') + N_2(X\ ^1\Sigma_g^+,\ v''),$$

the suppression of emission from the higher vibrational levels may be more severe than suggested by Green and Barth.[98]

The Lyman-Birge Hopfield band system of N_2. The Lyman-Birge-Hopfield band system arises from the a $^1\Pi_g$ - X $^1\Sigma_g^+$ transition in N_2, which proceeds through magnetic dipole and electric quadrupole radiation. The rate of population by electron impact is illustrated in Figures 14 and 15.

An additional source is provided by cascading from higher levels and in particular from transitions originating in the h $^1\Sigma_u^+$ and b $^1\Pi_u$ states. According to Green and Barth,[98] the total intensity may be increased by cascading by a factor of nearly five, whereas our calculations suggest an increase of about two. According to the measurements of Holland,[72] the enhancement does not exceed 40 percent and may be as little as 5 percent.

Green and Barth remark that the emission of the Lyman-Birge-Hopfield system is unaffected by deactivation, but this may not be the case. The emission from the higher vibrational levels could be suppressed by a vibrational interchange process similar to that noted for the A $^3\Sigma_u^+$ state. Without more precise data on vibrational deactivation processes, the prediction of individual band intensities is subject to serious uncertainty.

Other band systems. Other band systems will also appear in the dayglow. There are no measurements of the cross sections for the excitation of the b $^1\Pi_u$ and h $^1\Sigma_u^+$ states of N_2, and the predicted dayglow intensities of the resulting Birge-Hopfield, Janin, Watson-Koontz, and Herman-Gaydon band systems are largely arbitrary. We find with our assumed cross sections a combined overhead intensity of 2 kilorayleighs compared with the value of 10 kilorayleighs calculated by Green and Barth[98] for an overhead sun. The altitude profiles are similar to that for the C $^3\Pi_u$ state.

Similar uncertainties attend the prediction of the intensities of the first and second negative band systems of O_2. We obtain 400 Rayleighs above 120 km, about half the intensity above 120 km calculated by Green and Barth[98] for an overhead sun. The altitude profiles and intensities in the atmosphere will be modified by fluorescence.[30,123]

(2) Carbon Atoms in the Upper Atmosphere of Venus

The detection of carbon atoms in the upper atmosphere of Venus is reported in the present note which contains the results of an analysis performed on low resolution spectra of the planet Venus measured by Moos, et al.[129] for the spectral region λλ 1200-1900Å. This experiment

was performed in order to observe the 1216Å (Lyman-α) resonance line of atomic oxygen, and the longer wavelength albedo of the planet Venus. The spectra were obtained by employing an object prism telescope which operated from an accurately pointed Aerobee rocket platform at high altitudes in the earth's atmosphere. The derived data points are shown as open circles in Figure 16 as indicated in the legend. Moos, et al.[129] interpreted these spectra in terms of an 18 kR brightness signal for H I as well as evidence for the existence of O I in the upper atmosphere of Venus due to the observed spectral feature around 1300Å. Owing to the presence of both significant background fluctuations as well as the relatively weak nature of the signal involved, Moos, et al.[129] were able only to present a crude estimate of between 2 to 20 kR for the signal brightness of this O I spectral feature. However, the nominal assigned value of 11 kR[129] has been adopted for the purposes of the present analysis. Finally, it was concluded by Moos, et al.[129] that an anomalously high albedo of about 10^{-3} is indicated by the longer wavelength data. However, owing both to the relatively poor resolution in this spectral region and several experimental difficulties, no satisfactory explanation was presented for this emission feature.[129]

In the present investigation, a reinterpretation of the published spectra over the wavelength region $\lambda\lambda$ 1600-1900Å is presented in an attempt to identify emission features consistent with the published observations. For this purpose, three logical sources of emission for a solar-illuminated Venus atmosphere were considered: (a) Rayleigh scattering, (b) resonance-fluorescence from photochemically produced CO, (c) resonance emission from neutral carbon atoms at 1560 and 1657Å. In each case, theoretical estimates were made of the spectral characteristics and signal brightness values

pertinent to the indicated experimental conditions. These data were then employed as input parameters for the generation of synthetic spectra predicated on the available instrumentation characteristics. Cogent comparison between the theoretical and observed spectra indicate that the longer wavelength data can be explained satisfactorily by the presence of a 14 kR C I signal at 1657Å.

The synthetic spectrum generated by employing an 18 kR H I signal, an 11 kR 1304Å signal, as well as Rayleigh scattering from a solar illuminated CO_2 atmosphere[130] is illustrated in curve 1 of Figure 16. These results demonstrate that the generated synthetic spectrum indeed duplicates the observed H I and O I features satisfactorily. In addition the requirement to identify and additional longer wavelength emission feature is also emphasized. Photochemical equilibrium calculations demonstrate[130] that the photodecomposition of a predominantly CO_2 atmosphere (i.e. Venus and Mars) would result in the generation of both an optically thick CO situation as well as the presence of C I in the upper atmosphere of these planets. In this regard, calculations were performed[130] in order to derive estimates for the brightness values of the individual bands in the Fourth Positive system of CO. It has been shown[131] that the most intense fluorescence bands reside in the spectral region λλ 1500-1800Å wherein upper limit brightness values of between 100 to 300 Rayleighs/band obtain.[131] The contribution from this source is shown by the synthetic spectrum labelled curve 2 wherein it is evident, that even for this upper limit case, the calculated brightness values are not sufficient to explain the observations.

In addition to photodissociation, a number of other processes can contribute to the production of neutral carbon atoms in the upper atmosphere

of Venus including dissociative recombination involving CO^+, predissociation of CO^*, photoelectron and/or proton impact processes, etc. Additionally, C I possesses resonance lines at 1560 and 1657Å where the pertinent solar fluxes are 1.9×10^{10} photons/cm^2 sec and 8.0×10^{10} photons/cm^2 sec, respectively.[132] For the case of C I, quantitative calculations could not be performed owing to the lack of relevant data. Instead, a curve fitting procedure was adopted wherein a number of synthetic spectra were generated by adjusting both the absolute and the relative brightness values of the two resonance lines of C I. It was concluded that the optimum data fit shown as curve 3 in Figure 16 was achieved by invoking a 14 kR 1657Å signal wherein the contribution from the 1560Å feature could be ignored. This is not too surprising in view of the fact that the f_{ik}-values are 0.1 and 0.09 for 1657 and 1560Å, respectively.[133] However, it should be stressed that, even for equal contributions of the two lines, the resultant synthetic spectrum would reside within the observed error bars shown in Figure 16. Finally, it is appropriate at this point to re-emphasize that the C I values quoted above were derived on the basis of a nominal value of 11 kR for the O I feature, the absolute value of which lies between 2 and 20 kR.[129] As such, a corresponding uncertainty for the deduced C I values also obtain.

On the basis of the results of the above analysis, it is suggested that the rocket experiment be repeated wherein optimum resolution is sought for the spectral region $\lambda\lambda > 1500$Å. It is predicted that the C I lines would indeed be more evident in the observed spectrum. Furthermore if the sensitivity was increased in addition, then the stronger members of the CO Fourth Positive band system would also be observed. In this

regard, it clearly follows that current state-of-the-art scanning spectrometers,[134] which are operated in a planetary fly-by mode possess sufficient sensitivity and high resolution to confirm the above speculations. Specifically, the presence of these features should constitute the subject matter of an interesting study of the Mariner 6 and 7 experimental observations performed along the planetary limb of Mars. However, due to the substantial decrease in the solar flux between Venus and Mars, the resultant signal intensities would be reduced by more than a factor of 10 owing to the convolution of a lower production rate as well as a reduced resonance-fluorescence efficiency. Finally, it is of some importance to note that the remaining disagreements between the synthetic and theoretical spectra in the vicinities of 1250 and 1360Å in Figure 16 can be explained by conjecturing on the presence of C I emissions at 1261, 1277 and 1280Å and the well-known O I emission at 1356Å, respectively.

III. QUARTERLY PROGRESS REPORT FOR HOURS WORKED IN THE PERIOD 1 JUNE 1969 THROUGH 30 AUGUST 1969

In compliance with the requirements of the subject contract, the following is an integrated tabulation of total hours worked by labor category and grade.

Labor Category	Labor Grade	Total Hours
*Junior Technician	2	72
*Technician Experimental Machinist	3	133
*Senior Technician Senior Experimental Machinist	4	26
*Junior Scientist Junior Engineer	5	
*Scientist Engineer	6	
Senior Scientist Senior Engineer	7	
Staff Scientist	8	
Principal Scientist	9	176
Group Scientist Group Engineer	10	574

*and other equivalent categories

Quarterly total.....981

REFERENCES

1. Cohen, E.R.,and J. W. M. DuMond, Revs. Mod. Phys. 37, 537 (1965).

   These values were adopted by the National Academy of Sciences and National Research Council in 1963.

2. Birge, R. T., Revs. Mod. Phys. 13, 233 (1941)

3. Cohen, E. R., J. W. M. DuMond, T. W. Layton, and J. S. Rollet, Revs. Mod. Phys. 27, 363 (1955).

4. Hagstrum, H. D., Revs. Mod. Phys. 23, 185 (1951).

5. Clarke, E. M., Can. J. Phys. 32, 764 (1954).

6. Cloutier, G. G., and H. I. Schiff, J. Chem. Phys. 31, 793 (1959).

7. Watanabe, K., F. F. Marmo and E. C. Y. Inn, Phys. Rev. 90, 155 (1953)

8. Watanabe, K., J. Chem. Phys. 22, 1564 (1954).

9. Nicholson, A. J. C., J. Chem. Phys. 39, 954 (1963).

10. Baer, P. and E. Miescher, Nature, 169, 581 (1952).

11. Miescher, E., Helv. Phys. Acta, 29, 135 (1956).

12. Tanaka, Y., J. Chem. Phys. 21, 562 (1953).

13. Tanaka, Y., Sc. Papers I.P.C.R. 39, 456 (1942).

14. Huber, K. P. Helv. Phys. Acta, 34, 929 (1961).

15. Dressler, K. and E. Miescher, Astrophys. J. 141, 1266 (1965).

16. Miescher, E., J. Mol. Spectrosc. 20, 130 (1966).

17. Al-Joboury, M. I. and D. W. Turner, J. Chem. Soc. 4434 (1964).

18. Turner, D. W. and D. P. May, J. Chem. Phys. 45, 471 (1966).

19. Samson, J. A. R., Physics Letters, December (1968).

20. Huber, K. P. Can. J. Phys. 46, 1691 (1968).

21. Lefebvre-Brion, H. and C. M. Moser, J. Chem. Phys. 44, 2951 (1966).

22. McNesby, J. R., J. Atmos. Sci. 26, 594 (1969).

23. Sagan, C. E., Radiation Res. 15, 174 (1961).

24. Warneck, P., J. Chem. Phys. 46, 502 (1967).

25. Gorden, R. and Ausloos, P., J. Chem. Phys. 47, 1799 (1967).

26. Field, F. H., J. Am. Chem. Soc. 83, 1523 (1961); Wexler, S., A. Lifshitz, and A. Quaffrochi, Advan. Chem. Ser. 58, 193 (1966); Wexler, S. and J. Marshall, J. Am. Chem. Soc. 86, 781 (1964).

27. Botter, R., V. H. Dibeler, J. Walker and H. M. Rosenstock, J. Chem. Phys. 45, 1298 (1966).

28. Brehm, B., Z. Naturforsch, 21a, 196 (1966).

29. Schoen, R. I., J. Chem. Phys. 37, 2032 (1962).

30. Dalgarno, A., Ann. Geophys., 20, 65-73 (1964).

31. Dalgarno, A., M. B. McElroy and J. C. G. Walker, Planet. Space Sci. 15, 331-345 (1967).

32. Fite, W. L. and R. T. Brackmann, Phys. Rev. 113, 815-816 (1959).

33. Rothe, E. W., F. L. Marino, R. H. Neynaber and S. M. Trujillo, Phys. Rev. 125, 582-83 (1962).

34. Smith, K., R. J. W. Henry and P. G. Burke, Phys. Rev., 157,51-68 (1967).

35. Stauffer, A. D. and M. R. C., McDowell, Proc. Phys. Soc. (London), 89, 289-298 (1966).

36. Tate, J. T., and P. T. Smith, Phys. Rev., 39, 270-277 (1932).

37. Craggs, J. D., R. Thorburn and B. A. Tozer, Proc. Roy. Soc. (London), A240, 473-483 (1957).

38. Lampe, F. W., J. L. Franklin and F. H. Field, J. Amer. Chem. Soc., 79, 6129-35 (1957).

39. Rapp, D., and P. G. Englander-Golden, J. Chem. Phys. 43, 1464 (1965).

40. Schram, B. L., F. J. de Heer, M. J. van der Wiel and J. Kistemaker, Physica, 31, 94-112 (1965).

41. Schram, B. L., H. R. Moustafa, J. Schutten and F. H. de Heer, Physica, 32, 734 (1966).

42. Stewart, D. T. and E. Gabathuler, Proc. Phys. Soc. (London), 72, 287-289 (1958).

43. Nishimura, H., J. Phys. Soc. Japan, 21, 1018-1019, (1966).

44. Nishimura, H., J. Phys. Soc. Japan, 24, 130-143 (1968).

45. Aarts, J. F. M., and F. J. de Heer, Physica (1968 - in press).

46. Rapp, D., and D. D. Briglia, J. Chem. Phys., 43, 1480-1489 (1965).

47. Schulz, G. J., and J. T. Dowell, Phys. Rev., 128, 174-177 (1962).

48. McGowan, J. W., E. M. Clarke, H. P. Hanson and R. F. Stebbings, Phys. Rev. Lett., 13, 620-622 (1964).

49. Hake, R. D. and A. V. Phelps, Phys. Rev., 158, 70-84 (1967).

50. Lassettre, E. N., S. M. Silverman, and M. E. Krasnow, J. Chem. Phys. 40, 1261-1265 (1964).

51. Silverman, S. M. and E. N. Lassettre, J. Chem. Phys., 40, 2922-2932 (1964).

52. Peterson, J. R., Atomic Collision Processes, Amsterdam, North-Holland Publishing Co. (1964).

53. Steward, D. T., Proc. Phys. Soc. (London), A64, 437-440 (1956).

54. Sheridan, W. F., O. Oldenberg and N. P. Carleton, "Excitation of Nitrogen by Controlled Proton and Electron Impact." Second Int'l Conference on Physics of Electronic and Atomic Collisions, Boulder, Colorado.

55. Hayakawa, S., and H. Nishimura, J. Geomag. Geoelect., 16, 72-74 (1964).

56. Davidson, G. and R. O'Neil, "Production of N_2 1-N (0,0) Radiation by 60 keV Electrons." Fourth Int'l. Conference on Physics of Electronic and Atomic Collisions, Quebec, Canada (1965).

57. McConkey, J. W. and J. D. Latimer, Proc. Phys. Soc., 86, 463-466 (1965).

58. McConkey, J. W., J. W. Woolsey and D. J. Burns, Planet. Space Sci., 15, 1332-1334 (1967).

59. Holland, R. F., Los Alamos Scientific Laboratory Report LA-3783 (1967).

60. Srivastava, B. N. and I. M. Mirza, Phys. Rev. 168, 86-88 (1968).

61. Aarts, J. F. M., and F. J. de Heer, Physica (1968 - in press).

62. Thieme, O., Z. Phys., 78, 412-422 (1932).

63. Langstroth, G. O., Proc. Roy. Soc. (London), A146, 166-177 (1934).

64. Herrmann, O., Ann. Physik, 25, 143-165 (1936).

65. Kishko, S. M., and M. I. Kuchinka, Opt. Spektrosk., 6, 378-379 (1959).

66. Zapesochnyi, I. P., and S. M. Kishko, Izv. Akad. Nauk SSSR, 23, 965-967 (1959).

67. Fink, V. E., and K. H.Welge, Z. Naturforsch., 19A, 1193-1201 (1964).

68. Zapesochnyi, I. P., and V. V. Skubenich, Opt. Spektrosk., 12, 83 (1966).

69. Jobe, J. D., F. A. Sharpton and R. M. St. John, J. Opt. Soc. Amer., 57, 106-107 (1967).

70. Burns, D. J., F. R. Simpson and J. W. McConkey, J. Phys. B. (Proc. Phys. Soc.) (1968--in press).

71. Williams, S. E., Proc. Phys. Soc. (London), A47, 420-423 (1935).

72. Holland, R. F., Los Alamos Scientific Laboratory Report LA-DC-9468 (1968).

73. Winters, H. F., J. Chem. Phys. 44, 1472-1476 (1966).

74. Engelhardt, A. G., A. V. Phelps and G. G. Risk, Phys. Rev., 135, A1566-1574 (1964).

75. Takayanagi, K. and T. Takahashi, Rept. Ionos. Space Res. Japan, 20, 357-373 (1966).

76. Miller, R. E., J. Mol. Spectrosc., 19, 185-191 (1966).

77. Lassettre, E. N. and M. E. Krasnow, J. Chem. Phys., 40, 1248-1255, (1964).

78. Silverman, S. M. and E. N. Lassettre, J. Chem. Phys., 40, 2922-2932 (1964).

79. Geiger, J. and W. Stickel, J. Chem. Phys. 43, 4535-4536 (1965).

80. Lassettre, E. N., F. M. Glaser, V. D. Meyer and A. Skerbele, J. Chem. Phys., 42, 3429-3435 (1965).

81. Meyer, V. D. and E. N. Lassettre, J. Chem. Phys., 44, 2535-2536 (1966).

82. Haas, R., Z. Phys., 148, 177-191 (1957).

83. Schulz, G. J., Phys. Rev. 116, 1141-1147 (1959).

84. Schulz, G. J., Phys. Rev., 125, 229-232 (1962).

85. Schulz, G. J., Phys. Rev., 135, A988-A994 (1964).

86. Schulz, G. J., and H. C. Koons, J. Chem. Phys., 44, 1297-1298 (1966).

87. Boness, M. J. W., and J. B. Hasted, Phys. Letters, 21, 526-528 (1966).

88. Andrick, D. and H. Ehrhardt, Z. Phys. 192, 99-106 (1966).

89. Chen, J. C. Y., J. Chem. Phys. 40, 3513-3520 (1964); J. Chem. Phys., 41, 3263-3264 (1964).

90. Fite, W. L. and R. T. Brackmann, Phys. Rev. 112, 1151-1156 (1958).

91. Fite, W. L., R. F. Stebbings, and R. T. Brackmann, Phys. Rev. 116, 356-357 (1959).

92. Seaton, M. J., Atomic and Molecular Processes, New York, Academic Press, 375-420 (1962).

93. Schulz, G. J. and R. E. Fox, Phys. Rev. 106, 1179-1181 (1957).

94. Stebbings, R. F., W. L. Fite, D. G. Hummer and R. T. Brackmann, Phys. Rev., 119, 1939-1945 (1960).

95. Seaton, J. J., Phys. Rev., 113, 814 (1959).

96. Smith, P. T., Phys. Rev., 36, 1293-1302 (1930).

97. Maier-Leibnitz, H., Z. Phys. 95, 499-523 (1935).

98. Green, A. E. S., and C. A. Barth, J. Geophys. Res., 72, 3975-3986 (1967).

99. Stewart, D. T., Private communication (1968).

100. Hoegy, W. R., J. P. Fournier, and E. G. Fontheim, J. Geophys. Res., 70, 5464-5468 (1965).

101. Dalgarno, A., McElroy, M. B. and R. J. Moffett, Planet. Space Sci. 11, 463-484 (1963).

102. Tohmatsu, T., Rept. Ionospheric Space Res. Japan, 18, 425-437 (1964).

103. Chubb, T. A., E. T. Byram, H. Friedman and J. E. Kupperian, Ann. Geophys. 14, 109-116 (1958).

104. Donahue, T. M. and W. G. Fastie, Space Research IV, Amsterdam, North-Halland Publishing Co., 304-324 (1963).

105. Fastie, W. G. and H. M. Crosswhite, Planet. Space Sci., 12, 1021-1026 (1964).

106. Fastie, W. G., H. M. Crosswhite and D. F. Heath, J. Geophys. Res. 69, 4129-4140 (1964)

107. Kaplan, S. A., V. V. Katyushina, and V. G. Kurt, Space Research V, 595-611 (1965).

108. Katyushina, V. V., Kosmich. Issled. Akad. Nauk SSSR, 3, 248-251 (1965).

109. Fastie, W. G., Planet. Space Sci., 16, 929-935 (1968).

110. Dalgarno, A., Ann. Geophys. 20, 65-73 (1964).

111. Kaplan, S. A. and V. G.Kurt, Kosmich. Issled. Akad. Nauk SSSR 3, 256-261 (1965).

112. Donahue, T. M., Planet. Space Sci., 13, 871-888 (1965).

113. Tohmatsu, T., Rept. Ionospheric Space Res. Japan, 19, 509-514 (1965).

114. Garstang, R. H., Proc. Cambridge Phil. Soc., 57, 115-120 (1961).

115. Shklovskii, I. S., Sov. Astron. A. J., 1, 130-132 (1957).

116. Brandt, J. C., Ap. J. 130, 228-240 (1959).

117. Hinteregger, H. E., L. A.Hall and G. Schmidtke, Space Research V, 1175-1190 (1965).

118. Bates, D. R. and A. Dalgarno, J. Atmos. Terrest. Phys. 5, 329-344, (1954).

119. Walker, J. C. G., J. Atmos. Sci., 22, 361-369 (1965).

120. Wallace, L., and M. B. McElroy, Planet. Space Sci., 14, 677-708 (1966).

121. Noxon, J. F., J. Geophys. Res., 69, 3245-3255 (1964).

122. Dalgarno, A., and J. C. G. Walker, J. Atmos. Sci., 21, 463-474 (1964).

123. Dalgarno, A. and M. B. McElroy, Planet. Space Sci., 14, 1321-1329 (1966).

124. Barth, C. A. and J. B. Pearce, Space Research VI, London, MacMillan and Co., pp. 381 (1966).

125. Nagy, A. F., and J. P. Fournier, J. Geophys. Res., 70, 5981-5982 (1965).

126. Nicholls, R. W., Ann. Geophys. 20, 144-181 (1964)

127. Hunten, D. M., and M. B. McElroy, Rev. Geophys., 4, 303-328 (1966).

128. Ching, B. K., G. R. Cook and R. A. Becker, J. Quant. Spectrosc. Radiat. Transfer, 7, 323-337 (1967).

129. Moos, H. W., W. G. Fastie and M. Bottema, Astrophysical J. 155, #3, Pt. 1, 887 (1969).

130. Marmo, F. F., GCA Technical Report No. GCA TR 68-7-N (1968)

131. Marmo, F. F., ICARUS (accepted for publication) 1969.

132. Rense, W. A., Space Astrophysics, McGraw Hill Publishing Co. (1961).

133. Wiese, W. L., M. W. Smith and B. M. Glennon, Atomic Transition Probabilities, Hydrogen through Neon NSRDS-NBS 4 (Government Printing Office, Washington, D. C.) 1 (1966).

134. Barth, C. A. Paper AAS68-184 Advances in the Astronautical Sciences. Advanced Space Experiments (Proceedings of an American Astronautical Conference, held September 1968 at Ann Arbor, Michigan), 25, 69-77 (1969).